Eur. Phys. J. A (2026) 62:55
https://doi.org/10.1140/epja/s10050-025-01693-4

THE EUROPEAN PHYSICAL JOURNAL A

Regular Article - Experimental Physics

Cross section measurements of large angle fragments production in the interaction of carbon ion beams with thin targets

The FOOT Collaboration

Y. Dong[1], I. Mattei[1], A. Alexandrov[2], B. Alpat[3], G. Ambrosi[3], S. Argirò[4,5], M. Barbanera[3], N. Bartosik[5], G. Battistoni[1], M.G. Bisogni[6,7], V. Boccia[8,2], F. Cavanna[5], P. Cerello[5], E. Ciarrocchi[6,7], N. D'Ambrosio[9], A. De Gregorio[10], G. De Lellis[8,2], A. Di Crescenzo[8,2], B. Di Ruzza[11,12], M. Dondi[13,14], M. Donetti[15], M. Durante[8,16,17], R. Faccini[18,10], V. Ferrero[5], C. Finck[19], E. Fiorina[5], M. Francesconi[2], M. Franchini[13,14], G. Franciosini[20,10], G. Galati[12,21], L. Galli[7], M. Ionica[3], A. Iuliano[2,8], K. Kanxheri[22,3], B. Kharpuse[5], A.C. Kraan[7], C. La Tessa[23,24], A. Lauria[8,2], E. Lopez Torres[25,5], T. Maggipinto[21,12], M. Magi[20,10], A. Manna[14,13], M. Marafini[26,10], S. Masci[9], M. Massa[7], C. Massimi[14,13], S. Mazzolani[27,3], A. Mengarelli[14], A. Mereghetti[15], R. Mirabelli[20,10], A. Moggi[7], M.C. Montesi[28,2], M.C. Morone[29,30], M. Morrocchi[6,7], S. Muraro[1], N. Pastrone[5], V. Patera[20,10], F. Pennazio[5], F. Peverini[3,22], C. Pisanti[14,13], P. Placidi[3,31], M. Pullia[15], F. Quattrini[18,32,10], L. Ramello[33,5], C. Reidel[16], R. Ridolfi[14,13], L. Sabatini[34], L. Salvi[3,22], C. Sanelli[34], O. Sato[35], S. Savazzi[15], L. Scavarda[36], A. Schiavi[20,10], C. Schuy[16], E. Scifoni[24], L. Servoli[3], G. Silvestre[3], M. Sitta[33,5], B. Spadavecchia[4,5], R. Spighi[14], E. Spiriti[34], L. Testa[18,10], V. Tioukov[2], S. Tomassini[34], F. Tommasino[24,37], M. Toppi[20,10,a], G. Traini[10], A. Trigilio[34], G. Ubaldi[13,14], A. Valetti[4,5], M. Vanstalle[19], M. Villa[13,14], U. Weber[16,38], R. Zarrella[14,13], A. Zoccoli[14,13], A. Sarti[20,10]

[1] INFN Section of Milano, Milano, Italy
[2] INFN Section of Napoli, Napoli, Italy
[3] INFN Section of Perugia, Perugia, Italy
[4] University of Torino, Department of Physics, Torino, Italy
[5] INFN Section of Torino, Torino, Italy
[6] University of Pisa, Department of Physics, Pisa, Italy
[7] INFN Section of Pisa, Pisa, Italy
[8] University of Napoli, Department of Physics "E. Pancini", Napoli, Italy
[9] Istituto Nazionale di Fisica Nucleare (INFN), Section of Gran Sasso National Laboratories, Assergi (L'Aquila), Italy
[10] INFN Section of Roma 1, Rome, Italy
[11] University of Foggia, Foggia, Italy
[12] Department of Physics, University of Bari, Bari, Italy
[13] University of Bologna, Department of Physics and Astronomy, Bologna, Italy
[14] INFN Section of Bologna, Bologna, Italy
[15] CNAO National Center for Oncological Hadrontherapy, Pavia, Italy
[16] Biophysics Department, GSI Helmholtzzentrum für Schwerionenforschung, Darmstadt, Germany
[17] Institute of Condensed Matter Physics, Technische Universität Darmstadt, Darmstadt, Germany
[18] University of Rome La Sapienza, Department of Physics, Rome, Italy
[19] Université de Strasbourg, CNRS, IPHC UMR 7871, F-67000 Strasbourg, France
[20] University of Rome La Sapienza, Department of Scienze di Base e Applicate per l'Ingegneria (SBAI), Rome, Italy
[21] INFN Section of Bari, Bari, Italy
[22] University of Perugia, Department of Physics and Geology, Perugia, Italy
[23] University of Miami, Radiation Oncology, Miami, FL, United States
[24] Trento Institute for Fundamental Physics and Applications, Istituto Nazionale di Fisica Nucleare (TIFPA-INFN), Trento, Italy
[25] CEADEN, Centro de Aplicaciones Tecnologicas y Desarrollo Nuclear, Havana, Cuba
[26] Museo Storico della Fisica e Centro Studi e Ricerche Enrico Fermi, Rome, Italy
[27] University of Camerino, Department of Physics, Camerino, Italy
[28] University of Napoli, Department of Chemistry, Napoli, Italy
[29] University of Rome Tor Vergata, Department of Physics, Rome, Italy
[30] INFN Section of Roma Tor Vergata, Rome, Italy
[31] University of Perugia, Department of Engineering, Perugia, Italy
[32] Specialty School of Medical Physics, Sapienza, Rome, Italy
[33] University of Piemonte Orientale, Department for Sustainable Development and Ecological Transition, Vercelli, Italy
[34] INFN Laboratori Nazionali di Frascati, Frascati, Italy
[35] Nagoya University, Department of Physics, Nagoya, Japan
[36] ALTEC, Aerospace Logistic Technology Engineering Company, Corso Marche 79, 10146 Torino, Italy

[37] University of Trento, Department of Physics, Trento, Italy
[38] Institute of Medical Physics and Radiation Protection (IMPS), University of Applied Sciences, Giessen, Germany

Received: 28 February 2025 / Accepted: 4 September 2025

Abstract The fragmentation cross sections of carbon ion beams with kinetic energies of 115–353 MeV/u impinging on thin targets of graphite (C), polyvinyl-toluene (C_9H_{10}) and PMMA ($C_5O_2H_8$) have been measured at 90° and 60° at the CNAO particle therapy center (Pavia, Italy). Two detection arms were positioned at two different angles to perform the measurement at 90° and 60°. The fragment species have been identified in charge (Z_{id} = H) and mass (M_{id} = ^{1}H, ^{2}H, ^{3}H) combining the information of the deposited energy in thin plastic scintillators, of the deposited energy in a thick LYSO crystal and of the fragments Time of Flight (ToF) measurement. The ToF was also used to compute the fragments measured kinetic energy. This work presents, for the first time, a comparison of the measured fragmentation cross sections with predictions from FLUKA Monte Carlo and Geant4 codes. Such a comparison has never been shown before at the beam energies involved in this study, particularly for large-angle fragment production. A complete reanalysis by the FOOT collaboration of already published elemental cross section on composite targets has been performed to compare data with Monte Carlo, improving the analysis strategy and systematics uncertainties evaluation. The kinetic energy at production of measured fragments has been completely redefined, together with the efficiencies computation. The new analysis strategy has been successfully validated against the Monte Carlo cross sections. The cross sections are presented as a function of the fragments kinetic energy at production thanks to an unfolding technique applied to the data.

1 Introduction

Particle Therapy (PT) is the external radiation therapy technique that exploits protons and carbon ion beams to treat especially deep-seated solid tumors close to organs at risk [1]. In particular, carbon ions are used to treat radio-resistant tumors thanks to their higher biological effectiveness in killing cancerous cells with respect to photons and protons [2], but nuclei with a mass number A > 1 may undergo fragmentation in the nuclear interaction with patients tissue nuclei. Heavy fragments will be produced at small angles with respect to the projectile incident direction, causing the dose tail beyond the Bragg peak, while light fragments such ^{1}H, ^{2}H and ^{3}H can be produced even at large angles, depositing their dose far from the beam trajectory. The knowledge of the production of Z = 1 fragments at large angles is also of interest for beam range monitoring techniques based on the detection of charged secondary fragments [3] and for radioprotection purposes on long term space missions [4,5]. Treatment plans based on simulations both with analytical and Monte Carlo (MC) approaches [6] suffer from the uncertainties on the Relative Biological Effectiveness (RBE) assessment, due to the large uncertainties on the knowledge of the production fragmentation cross section of 80–400 MeV/u ^{12}C ion beam, both at experimental level and in the related calculation models [7]. Several measurements with a detection angle below 45°, and only a small number of beam-target-energy combinations, have been performed by other research groups [8–14].

In this paper, the cross section measurements for the production of Z = 1 fragments (protons, deuterons and tritons), detected at large angles (90° and 60°), from the interaction of 115–353 MeV/u ^{12}C ion beams with a graphite (C), polyvinyl-toluene (EJ-212 from Scionix [15], CH in the following) and polymethyl-methacrylate (PMMA) targets are reported. The experimental data of the cross section of ^{12}C ion beam on carbon (C), oxygen (O) and hydrogen (H) elemental targets at large angle have been already published [16] by the FOOT collaboration [17], exploiting the composite targets subtraction method from the cross section of ^{12}C ion beam impinging on C, CH and PMMA targets, from a data taking performed at the CNAO therapy center (Pavia, Italy). In this work, the same dataset is reanalyzed, in order to show, for the first time, the comparison of measured data with the Monte Carlo predictions of the FLUKA and Geant4 codes. To this aim, the FOOT collaboration took the opportunity to improve the entire analysis strategy. Advancements have been made, in particular, in the efficiency computation, in the extraction of the kinetic energy through a new unfolding technique and in the systematic uncertainties evaluation. In Sect. 2 the experimental setup and configurations are described, in Sect. 3 the data analysis strategy is presented. The computation of the fragment kinetic energy at production has been implemented exploiting an unfolding technique of the measured fragment kinetic energy (see Sect. 3.1.1), while in the already published data an analytic function was applied for the measured kinetic energy correction. Moreover, instead of computing a fragment identifica-

Communicated by Jose Benlliure.

[a] e-mail: marco.toppi@uniroma1.it

Table 1 Targets composition and parameters [16]

Target	Composition	Thickness $[mm]$	th_Y $[mm]$	Density $[g/cm^3]$	A_Y $[u]$
Graphite	C	1	1.4	0.94	12.01
Polyvinyl	C_9H_{10}	2	2.8	1.024	118.18
PMMA	$C_5O_2H_8$	2	2.8	1.19	100.12

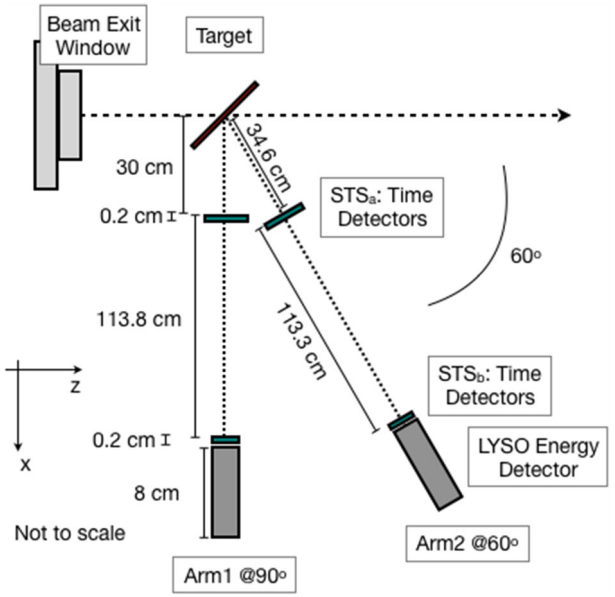

Fig. 1 Sketch of the experimental setup (not to scale) [16]

tion efficiency averaged on the kinetic energy at production of fragments, in the presented analysis the fragment identification efficiency is modulated as a function of the fragment production kinetic energy (see Sect. 3.2.2). The systematic uncertainty evaluation is discussed in Sect. 3.3. In Sect. 4 the results are reported and the comparison with FLUKA Monte Carlo and Geant4 codes [18–22] predictions is also shown for the first time and discussed in Sect. 5.

2 Experimental configurations

The double differential fragmentation cross sections of ^{12}C ion beam over low density graphite sheet (C), polyvinyltoluene (polyvinyl in Table 1 – CH) and PMMA thin targets (see Table 1) have been measured in air, in clinical like conditions, exploiting five beam energies: 115 MeV/u, 150 MeV/u, 221 MeV/u, 279 MeV/u and 351 MeV/u. The beam intensity was the therapeutical one ($\sim 10^8$ ions/s). Each target, with atomic mass number A_Y, was placed at 45° with respect to the incoming beam direction ($th_Y = Thickness \cdot \sqrt{2}$), and was impinged by $\sim 5 \times 10^{10}$ ions.

The experimental setup is shown in Fig. 1: at 90° and 60°, two detection arms (Arm1 and Arm2) were placed for the detection of secondary charged fragments. In each arm, two thin plastic scintillators, 2 mm thick (STS_a and STS_b), were used for the Time of Flight (ToF) and energy loss measurement of the fragments with a 0.59 ns and 0.43 ns ToF resolution for Arm1 and Arm2 respectively, as reported in [16]. Such resolutions lead to a velocity uncertainty ranging from 5% at 50 MeV/u to 10% at 320 MeV/u, and hence to a kinetic energy uncertainty ranging between 10% and 20%. A LYSO crystal $4 \times 4 \times 8$ cm^3 was used as calorimeter for the fragments kinetic energy measurements. The Data AcQuisition (DAQ) trigger was the logic OR of the trigger of Arm1 and Arm2. The trigger of Arm1(2) was the logic AND of the STS_a and STS_b discriminated signals of Arm1(2) (more details on the experimental setup are given in [16]). For each trigger, the fragments considered for the analysis are the ones whose correspond to an energy release in both the STSs and in the LYSO.

3 Methods

The double differential cross section computed as a function of the fragment kinetic energy at production (E_k) and measured at $\theta = 60°, 90°$ is defined as:

$$\frac{d^2\sigma}{d\Omega dE_k}\left({}^A_Z X\right) = \frac{N_{{}^A_Z X}(E_k)}{N_Y\ \Delta\Omega\ \Delta E_k\ N_{^{12}C}\ \epsilon\,(E_k)}. \tag{1}$$

$N_{{}^A_Z X}(E_k)$ is the number of fragments with a specific atomic number Z and mass number A, in each kinetic energy bin E_k; N_Y is the number of scattering centers per unit surface; $\Delta\Omega$ is the solid angle of the fragments at production seen and reconstructed by the LYSO detector; ΔE_k is the fragment kinetic energy bin size; $N_{^{12}C}$ is the number of incoming carbon ions and $\epsilon(E_k)$ is the total efficiency.

The number of scattering centres in a Y target per unit surface is defined as:

$$N_Y = \frac{\rho_Y \cdot th_Y \cdot N_A}{A_Y} \tag{2}$$

where A_Y is the atomic mass number, N_A the Avogadro number, ρ_Y the target density and th_Y is the thickness of the crossed target (see Table 1). $\Delta\Omega$ has been computed by means of the MC simulation, taking into account the spatial distribution of the beam and the multiple scattering underwent by fragments before reaching the LYSO detector. The

number of carbon ions $N_{^{12}C}$ is provided by the CNAO dose delivery system from the released charge measured by ionization chambers. A 4% relative uncertainty on $N_{^{12}C}$ is related to the current measurement precision and to the dose-current conversion systematic uncertainty [23–25] and it has been accounted in the final result as a systematic uncertainty.

The total efficiency $\epsilon(E_k)$ is factorized in three terms, each one depending on the production kinetic energy:

$$\epsilon(E_k) = \epsilon_{Rec} \cdot \epsilon_{PID} \cdot \epsilon_{DT} \tag{3}$$

where ϵ_{Rec} includes the geometrical, trigger and detection efficiency of Z = 1 fragment (see Sect. 3.2.1), ϵ_{PID} is the particle identification efficiency (see Sect. 3.2.2) and ϵ_{DT} is the dead time efficiency, in order to take into account for the DAQ dead time, which depends on the beam rate and was measured to be in the 2–8% range, as reported in [16]. To evaluate ϵ_{Rec} and ϵ_{PID} and other corrections defined in the following sections, FLUKA MC simulations of the geometrical setup have been performed, one for each target type and beam energy.

3.1 Fragment identification

The number of specific fragments, $N_{^A_Z X}$ as a function of E_k, *i.e.* the fragment kinetic energy at production, is evaluated following the equation:

$$N_{^A_Z X}(E_k) = \boldsymbol{U} \cdot \left(N_{^A_Z X}\left(E_k^m\right) \cdot p\left(E_k^m\right) \right) \tag{4}$$

where $\boldsymbol{U}$ is the unfolding matrix (see Sect. 3.1.1), $p(E_k^m)$ is the *purity* (see Eq. 5), $N_{^A_Z X}(E_k^m)$ is the number of $^A_Z X$ fragment as a function of the measured kinetic energy:

$$E_k^m = m_i c^2 \cdot (\gamma_i - 1)\,;$$

with

$$\gamma_i = \left(1 - \beta_i^2\right)^{-1/2} \quad , \quad \beta_i = L/\left(ToF_i \cdot c\right).$$

m_i is the mass of the fragment $i = p, d, t$, L is the distance between STS_a and STS_b, c is the speed of light and ToF_i is the measured time of flight of the i fragment.

The number of $^A_Z X$ fragments has been evaluated after the particle identification (PID) in charge Z and mass A, following the same procedure described in [16]: to identify the fragment charge (Z = 1), the information on the energy released in the STSs, by means of a charge-to-digital converter (QDC) module (CAEN V792), has been combined with the LYSO QDC and ToF measurement; the fragment mass (A = 1,2,3) has been identified combining the LYSO QDC with the measurement of 1/ToF. Due to the low statistics, results are shown neither for pions, which are only present in a small fraction at the higher carbon ion beam energies (above 280 MeV/u), nor for Z = 2 charged fragments, which occur in less than 2% of the cases at 60° [16].

Once $N_{^A_Z X}(E_k^m)$ has been evaluated, it has been corrected for the *purity*. As described in [16], the same PID algorithm has been implemented in the MC simulation using the Energy and ToF experimental resolution to tune the MC response to data. *Purity* has been computed thanks to the FLUKA Monte Carlo simulation of the full geometrical setup for each target-beam configuration and it is defined as:

$$p(E_k^m) = \frac{N_{^A_Z X}^{MC}\left(E_k^m\right)_{PID}}{N_{^A_Z X}^{recoMC}\left(E_k^m\right)_{PID}}. \tag{5}$$

E_k^m is the kinetic energy obtained by ToF, as in experimental data, $N_{^A_Z X}^{MC}(E_k^m)_{PID}$ is the number of correctly identified $^A_Z X$ fragments and $N_{^A_Z X}^{recoMC}(E_k^m)_{PID}$ is the number of reconstructed $^A_Z X$ fragments after identification. *Purity* values range between 95% and 100%. Clearly, the discrepancies between data and MC response are a source of systematic effects which enter both in PID and purity corrections. These contributions have been included in the overall systematic uncertainty and will be discussed in detail in Sect. 3.3.

3.1.1 Unfolding of measured kinetic energy

After the *purity* correction, to obtain the number of $^A_Z X$ fragment as a function of the kinetic energy of the fragment at production ($N_{^A_Z X}(E_k)$ in Eq. 4), an unfolding technique, based on the *RooUnfoldBayes* method of the RooUnfold package [26] based on the ROOT software [27], has been applied to the measured kinetic energy spectrum, due to the fact that a fragment loses energy before exiting the target and in air before being detected. The unfolding matrix $\boldsymbol{U}$ has been computed from a MC simulation of the geometrical setup reproducing each experimental configuration of beam energy-target type. The unfolding matrix, gives the probability that a fragment with a measured kinetic energy had a certain production energy. The $\boldsymbol{U}$ matrix is then applied to the measured fragment yields $^A_Z X$, reconstructed in bin of kinetic energy, to obtain the fragment yields $^A_Z X$ in bin of production kinetic energy. As an example of the result, in Fig. 2 left, it is shown the matrix for the case of protons produced in PMMA and detected by Arm1 (90°). In Fig. 2 right, the unfolding matrix is applied to the Monte Carlo measured kinetic energy spectrum of reconstructed protons (blue circles), obtained from the MC simulation of the setup used also to compute the *purity*. The unfolded energy spectrum (black triangles) is therefore obtained and compared to the kinetic energy spectrum at production (red squares). The unfolding parameter

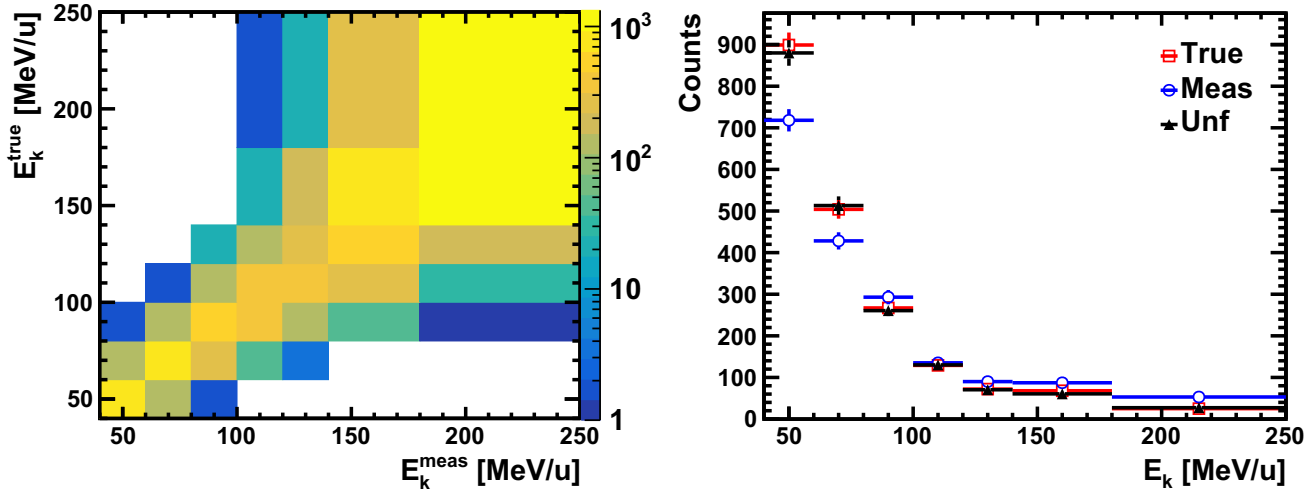

Fig. 2 Left: unfolding matrix $\boldsymbol{U}$ of E_k as a function of E_k^{meas}, obtained from a full MC simulation, for the case of protons detected at 90° and produced by a 351 MeV/u ^{12}C ion beam impinging on the PMMA target. Right: tuning of the unfolding procedure. The unfolding matrix (left) is applied to the MC reconstructed protons distribution (blue circles) in order to obtain the unfolded distribution (black triangles). The unfolded kinetic energy at production has to be compared to the MC protons kinetic energy at production (red squares)

of the *RooUnfoldBayes* method, which is the number of the unfolding iteration *niter*, is tuned exploiting the MC distributions as described, minimizing the χ^2 between the true and the unfolded MC distributions.

3.2 Efficiency evaluation

3.2.1 Detection efficiency

The detection efficiency is the convolution of geometrical, trigger and detection efficiencies. It has been computed as a function of the fragment kinetic energy at production, following the equation:

$$\epsilon_{Det}(E_k) = \frac{N_{{}^A_Z X}^{recoMC}(E_k)_{TE}}{N_{{}^A_Z X}^{trueMC}(E_k)_{\Delta\Omega}} \tag{6}$$

where $N_{{}^A_Z X}^{recoMC}(E_k)_{TE}$ is the number of ${}^A_Z X$ fragments MC reconstructed as experimental data after the trigger selection (T) and detectors energy thresholds cuts (E: 100 keV for STSs and 12 MeV for LYSOs). No PID is used at this level, the fragment identification is done at MC generator level. The trigger is defined in simulation in the same way as in experimental data acquisition, that is the time coincidence between the two STSs. The same is done for energy threshold cuts, implemented in the MC analysis as they are in experimental data. $N_{{}^A_Z X}^{trueMC}(E_k)_{\Delta\Omega}$ is the number of generated ${}^A_Z X$ fragments produced in the $\Delta\Omega$ seen by the LYSO detector. The denominator of the detection efficiency corresponds to the MC prediction of the yield of the produced fragment ${}^A_Z X$ to be compared with the measured experimental data (see Sect. 4).

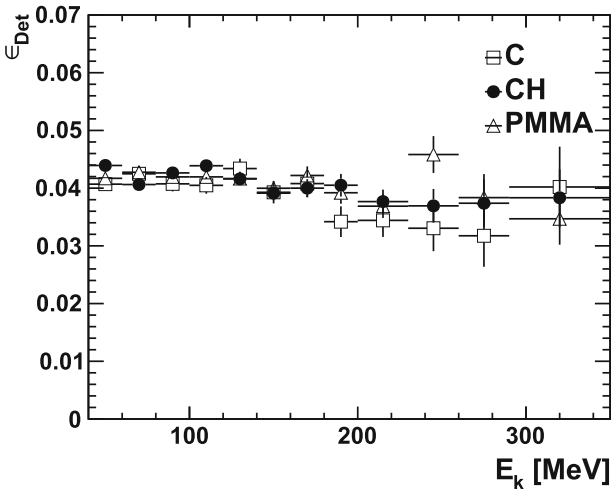

Fig. 3 Detection efficiency (convolution of geometrical, trigger and detection efficiencies) as a function of the kinetic energy at production of the detected proton fragments. The shown efficiency is computed from the FLUKA MC simulation of the 351 MeV/u ^{12}C ion beam impinging on C, CH and PMMA targets, with fragments detected at 60°

An example of the obtained $\epsilon_{Det}(E_k)$ for secondary proton fragments detected at 60° is shown in Fig. 3 for the case of the 351 MeV/u ^{12}C ion beam impinging on C (open square), CH (full circle) and PMMA (open triangle) targets. No dependency of the efficiency to the target type is observed. The small absolute value is mostly due to the multiple scattering underwent by large angle emitted secondary fragments from the target exit to the LYSO crystal.

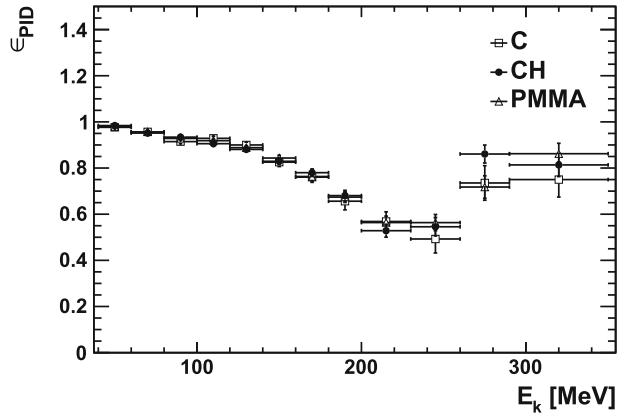

Fig. 4 Particle identification efficiency ($\epsilon_{PID}(E_k)$) as a function of the kinetic energy at production of the detected proton fragments. The shown efficiency is computed from the FLUKA MC simulation of the 351 MeV/u ^{12}C ion beam impinging on C, CH and PMMA target, with secondary protons detected at 60°

3.2.2 Particle identification efficiency

The particle identification efficiency (ϵ_{PID}) has been computed as a function of the reconstructed ${}^{A}_{Z}X$ fragment kinetic energy at production, with the following equation:

$$\epsilon_{PID}(E_k) = \frac{N^{recoMC}_{{}^{A}_{Z}X}(E_k)_{PID}}{N^{recoMC}_{{}^{A}_{Z}X}(E_k)_{TE}} \tag{7}$$

where $N^{recoMC}_{{}^{A}_{Z}X}(E_k)_{PID}$ is the number of MC fragments reconstructed in Z and A after the particle identification selection (see Sect. 3.1), implemented as it is in experimental data, while $N^{recoMC}_{{}^{A}_{Z}X}(E_k)_{TE}$ is the same as the numerator of $\epsilon_{Det}(E_k)$ (see Sect. 3.2.1). In Fig. 4 the result of ϵ_{PID} for the identified proton fragments (ϵ^{p}_{PID}) is reported for the case of MC simulation of 351 MeV/u ^{12}C ion beam impinging on C (open square), CH (full circle) and PMMA (open triangle) target and proton fragments detected at 60°.

The trend of ϵ^{p}_{PID} is due to the PID selection functions, that are done on the experimental data distribution of the deposited energy in LYSO (*Eloss* in terms of LYSO QDC) as a function of 1/ToF, with ToF the fragments time of flight (see Sect. 3.1). The decreasing of ϵ^{p}_{PID} is due to secondary fragments that, only for geometrical reasons, are not fully contained by the LYSO detector, depositing an energy that is cutted out by the lowest *Eloss* vs 1/ToF selection function. On the other hand, the increasing of the PID efficiency after 215-245 MeV/u is due to the fact that, when the kinetic energy of a particle exceeds a certain energy, the energy lost by that particle in the detector decreases as 1/ToF increases: the particle "punches through" the LYSO detector, decreasing its *Eloss* and re-entering the highest selection cut. This effect is accurately reproduced by the Monte Carlo simulation, thanks to the MC distribution of the deposited energy in LYSO that has been tuned in order to reproduce the shape of the LYSO QDC of experimental data. This effect is taken into account by ϵ_{PID}, with the corresponding systematic uncertainty sys_{PID} highlighting its impact (as described in Sect. 3.3).

3.3 Systematic uncertainty evaluation

A crucial aspect in the evaluation of the results (see Sect. 4) is the assessment of the systematic uncertainty, that, in this analysis, is computed as a function of the fragment kinetic energy at production. The systematic uncertainty in the cross section measurement (as defined in Eq. 1) originates from the following main sources:

1. Unfolding procedure (sys_{unf})
2. $\Delta\Omega$ evaluation from MC simulation ($sys_{\Delta\Omega}$)
3. Particle identification selections (sys_{PID})
4. Evaluation of the number of incoming ions $N_{^{12}C}$ (relative systematics 4%).

The dominant contribution comes from the unfolding procedure used to correct the measured kinetic energy to the production kinetic energy. This contribution has been evaluated within MC, even using a different unfolding technique (*RooUnfoldIDS* instead of *RooUnfoldBayes*) and its impact ranges between 0.1% and 13% for the most populated bins. This systematics in the previous published work [16] was completely underestimated, reminding that the energy correction in that work had been done with an analytic function. sys_{unf} is also the main source of uncertainty in the differential cross sections.

The second contribution to the systematic uncertainty comes from the evaluation of $\Delta\Omega$. $\Delta\Omega$ is computed by exploiting the MC simulation, taking into account the reconstructed fragments, since no tracking system is present in the experimental setup (see Fig. 1). $\Delta\Omega$ affects the cross section normalization and the detection efficiency evaluation, as shown in Eqs. 1 and 6. Therefore, the impact of the $\Delta\Omega$ choice in the MC influences the final cross section results. For this reason, $\Delta\Omega$ has been varied from the default value and evaluated its impact on the systematic uncertainty $sys_{\Delta\Omega}$. This ranges from 1% up to 14% for the most populated bins.

The systematic uncertainty on the differential cross section due to the PID selection (sys_{PID}) has been evaluated by varying of 1% the PID selection functions. The relative error due to this systematics ranges between 0.1% up to 6%, depending on the fragment kinetic energy bin. The PID systematics has an impact in the fragment yields (see Eq. 1 and Sect. 3.1), in the *purity* (see Eq. 5) and in the PID efficiency evaluation (see Eq. 7). The higher the fragment kinetic

energy at production, the higher the relative systematics due to this source of uncertainty, as expected due to the bigger discrepancies between the PID selection bands and the *Eloss* vs 1/ToF distributions at high energy.

4 Results

The results on the double differential cross section (DDCS in the following figures) of protons detected at 90° and 60°, produced by the nuclear fragmentation of ^{12}C ion beams of 115–351 MeV/u kinetic energy impinging over composite targets of C, CH and PMMA computed as described by Eq. 1, are shown as black squares, respectively, in Figs. 5, 6,

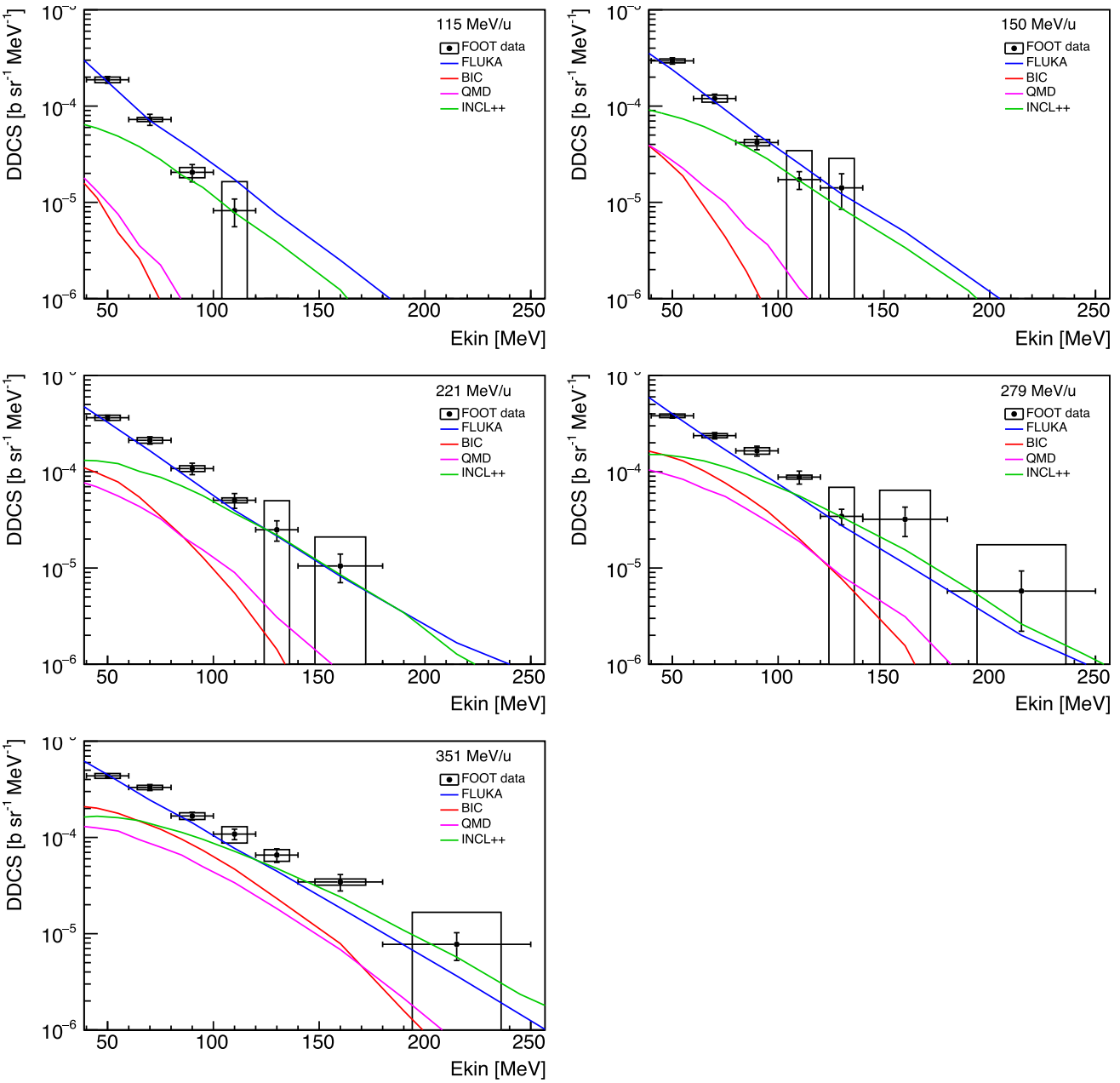

Fig. 5 Double differential cross section as a function of fragment kinetic energy for proton fragments detected at 90°, produced in the nuclear interaction of 115-351 MeV/u carbon ion beam with a graphite target. The statistical uncertainty (cross) and systematic uncertainty (empty square) on experimental data are shown as separate contributions

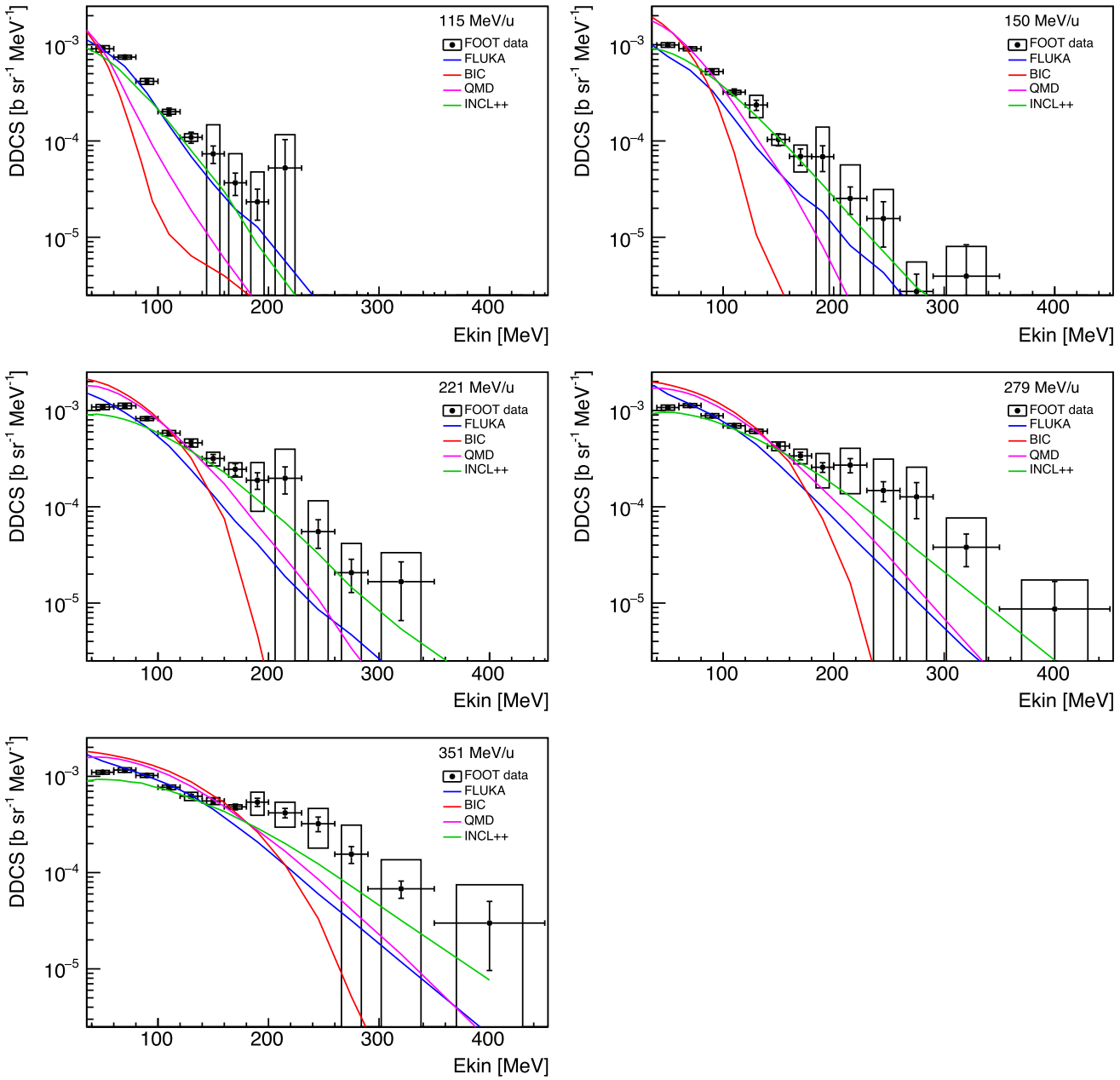

Fig. 6 Double differential cross section as a function of fragment kinetic energy for proton fragments detected at 60°, produced in the nuclear interaction of 115-351 MeV/u carbon ion beam with a graphite target. The statistical uncertainty (cross) and systematic uncertainty (empty square) on experimental data are shown as separate contributions

7, 8, 9 10. The statistical uncertainty (cross) and systematic uncertainty (empty square) on the measurements are shown as separate contributions. The values of the differential cross section (DCS in the following figures), integrated in energy between E_k = 40–250 MeV/u at 90° and E_k = 40–350 MeV/u at 60°, are also shown as a function of the primary beam energy for the three targets (C – left panel, CH – middle panel and PMMA - right panel), for protons (p), deuterons (d) and tritons (t), detected at 90° (Fig. 11) and 60° (Fig. 12). The FLUKA MC prediction is superimposed to the experimental data as blue line in all figures. For the case of protons produced by the interactions with the graphite target, together with the FLUKA model, also the BIC, INCL++ and QMD Geant4 models are superimposed. The reported error in the simulation results is purely statistical. Numerical values are reported in the tables shown in Appendix A.

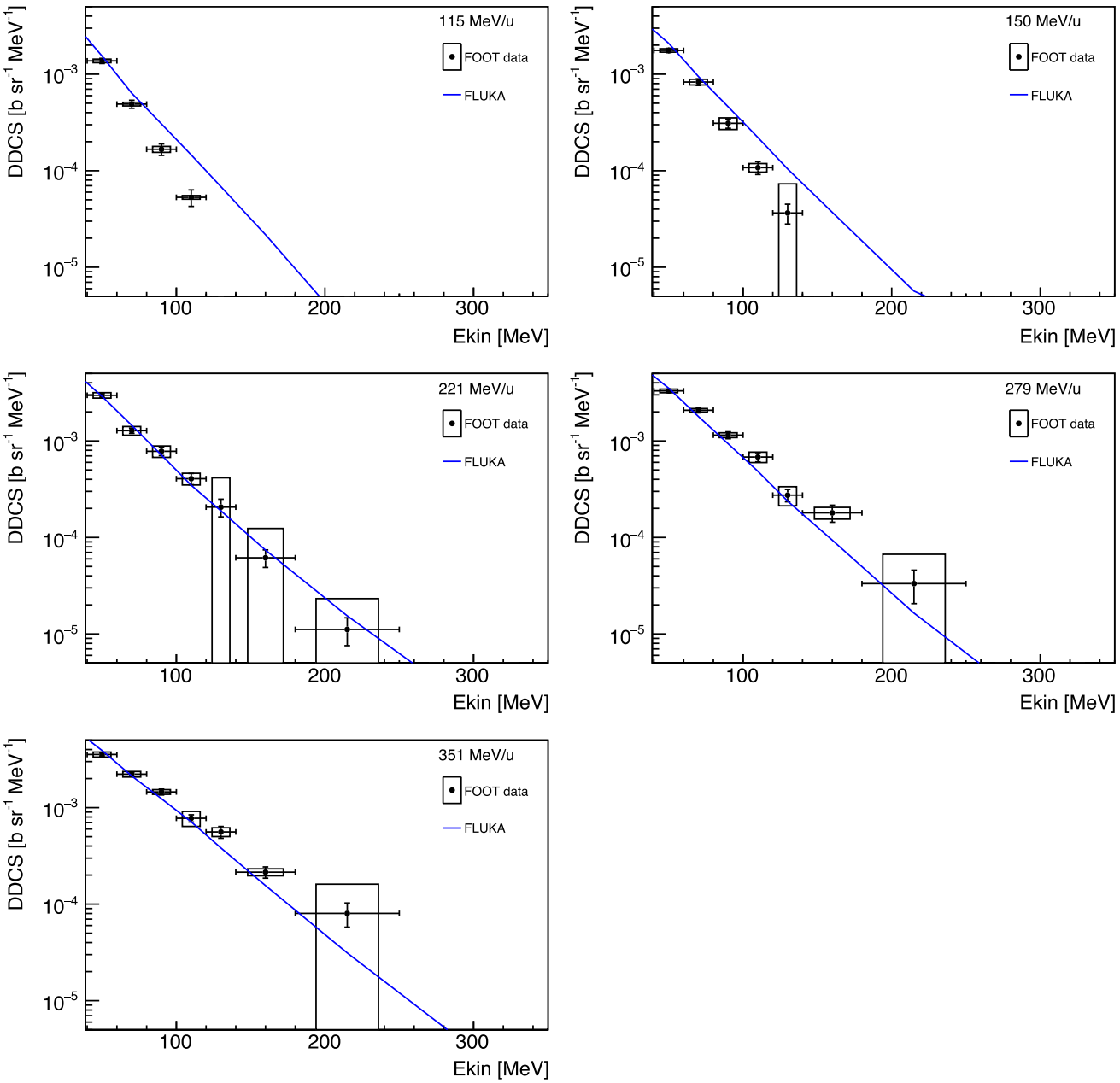

Fig. 7 Double differential cross section as a function of fragment kinetic energy for proton fragments detected at 90°, produced in the nuclear interaction of 115-351 MeV/u carbon ion beam with a polyvinyl-toluene target. The statistical uncertainty (cross) and systematic uncertainty (empty square) on experimental data are shown as separate contributions

The MC prediction results on the double differential cross section are computed with the following formula:

$$\frac{d^2\sigma^{MC}}{d\Omega dE_k}\left({}^{A}_{Z}X\right) = \frac{N^{trueMC}_{{}^{A}_{Z}X}\,(E_k)_{\Delta\Omega}}{N_Y\;\Delta\Omega\;\Delta E_k\;N^{MC}_{^{12}C}} \tag{8}$$

where the numerator, shown also in Eq. 6, is the number of generated ${}^{A}_{Z}X$ fragments produced in the $\Delta\Omega$ seen by the LYSO detector, N_Y, $\Delta\Omega$ and ΔE_k are the same quantities described in Eq. 1 and $N^{MC}_{^{12}C}$ is the number of simulated carbon ions impinging the target ($\sim 10^{10}$ (FLUKA), 10^8 (Geant4) primary ions for each simulated target - beam configuration). The analysis strategy and the FLUKA MC corrections applied to the cross section formula (see Eq. 1) have been validated comparing the FLUKA MC production cross section, in Eq. 8, with the FLUKA MC reconstructed one, computed following Eq. 1.

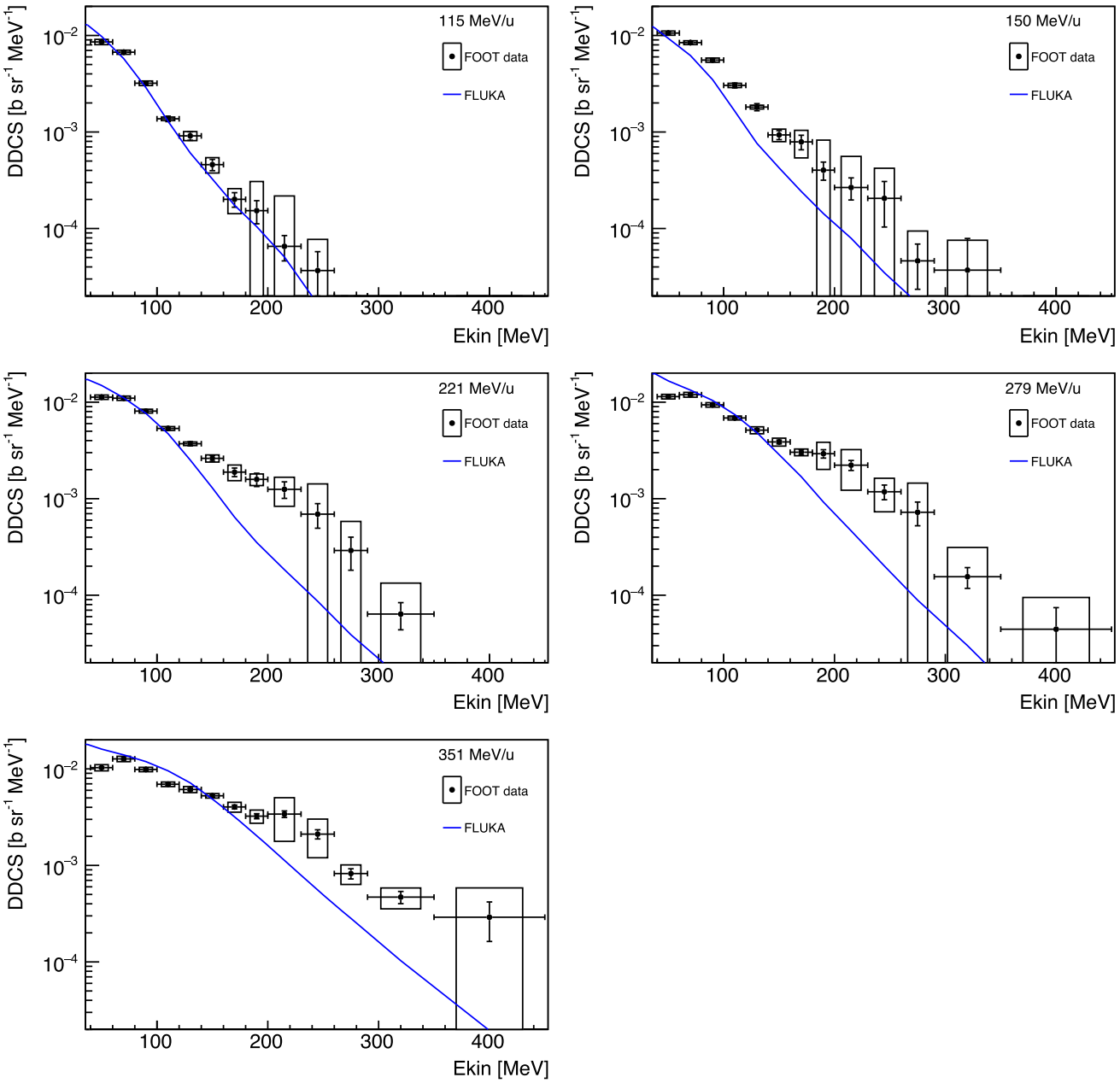

Fig. 8 Double differential cross section as a function of fragment kinetic energy for proton fragments detected at 60°, produced in the nuclear interaction of 115–351 MeV/u carbon ion beam with a polyvinyl-toluene target. The statistical uncertainty (cross) and systematic uncertainty (empty square) on experimental data are shown as separate contributions

As far as deuterons and tritons are concerned, since their yield at large angle is very low, the available statistics is low and only the energy integrated differential cross sections, in the same energy interval of protons, as a function of the ^{12}C ion beam kinetic energy in Figs. 11 and 12 can be presented. Again, statistical (cross) and systematic uncertainties (empty square) on experimental data (black squares) are shown as separate contributions, and the FLUKA MC predictions are superimposed as blue line. For the case of the interactions with the graphite target, together with the FLUKA model, also the BIC, INCL++ and QMD Geant4 models are superimposed.

5 Discussion and conclusions

This work is devoted to the study of the emission of nucleons and light charged fragments at large polar angle in ^{12}C

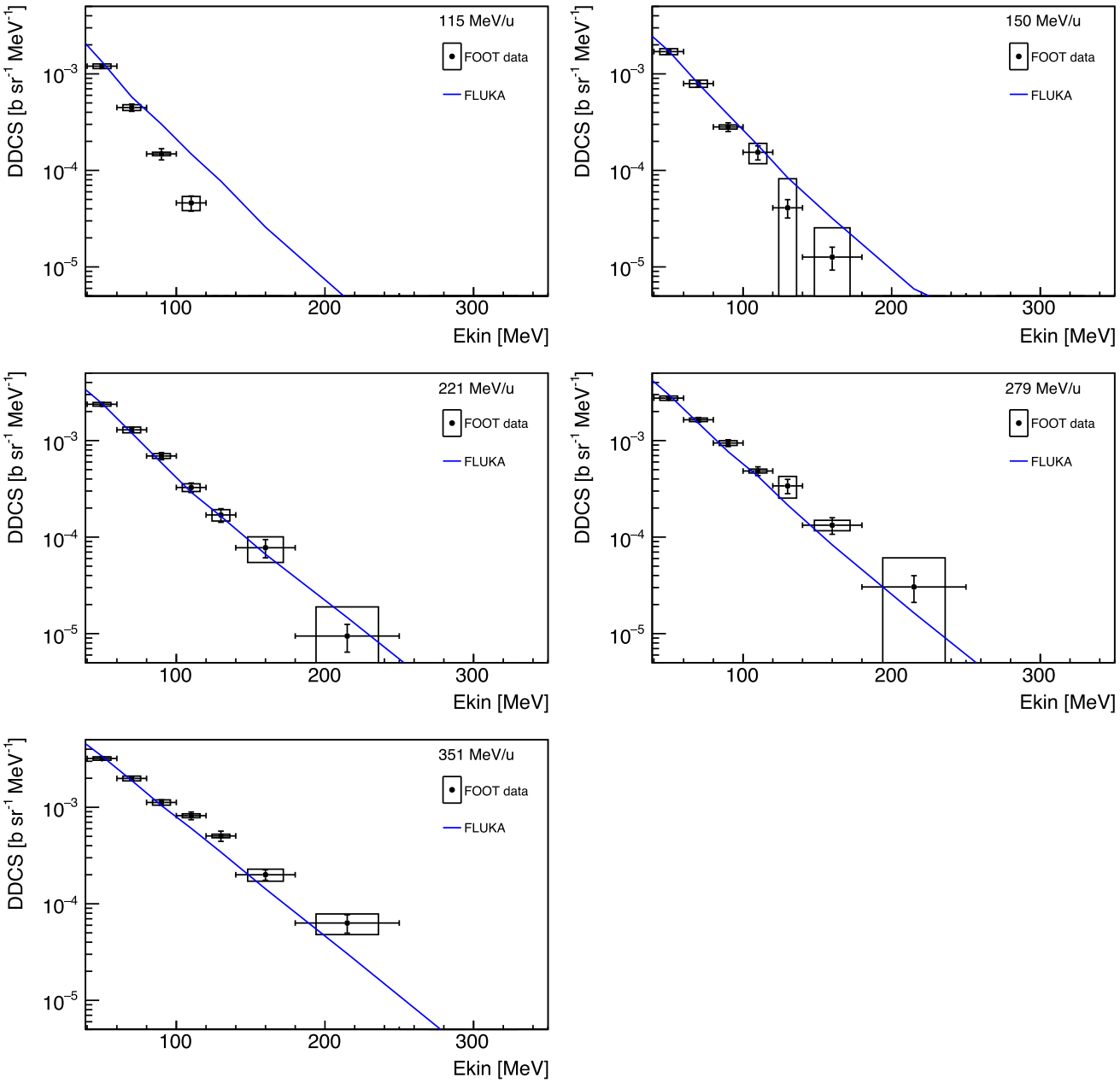

Fig. 9 Double differential cross section as a function of kinetic energy for proton fragments detected at 90°, produced in the nuclear interaction of 115–351 MeV/u carbon ion beam with a PMMA target. The statistical uncertainty (cross) and systematic uncertainty (empty square) on experimental data are shown as separate contributions

collisions in the energy range used in particle therapy. The main aim is to provide data to benchmark the models used for specific tasks, as those concerning range monitoring in ion therapy by means of the detection of light nuclear fragments emitted by the interaction of the therapeutic beam in the patient [3,28,29]. There have been other works in the past where data on yield at large angle from thick targets have been measured [30–33], but no cross section measurements on thin target have been published other than Ref. [16].

In the present work, the double differential cross sections of protons produced at large angles (60 and 90 degrees) from the nuclear interaction of ^{12}C ion beams of 115–351 MeV/u impinging over graphite, polyvinyl-toluene and PMMA targets are presented, together with the energy integrated differential cross section for ^{2}H and ^{3}H isotopes. For the first time, a comparison with the predictions obtained from the FLUKA MC code and three Geant4 models is also shown. These results are obtained from a complete novel analysis of

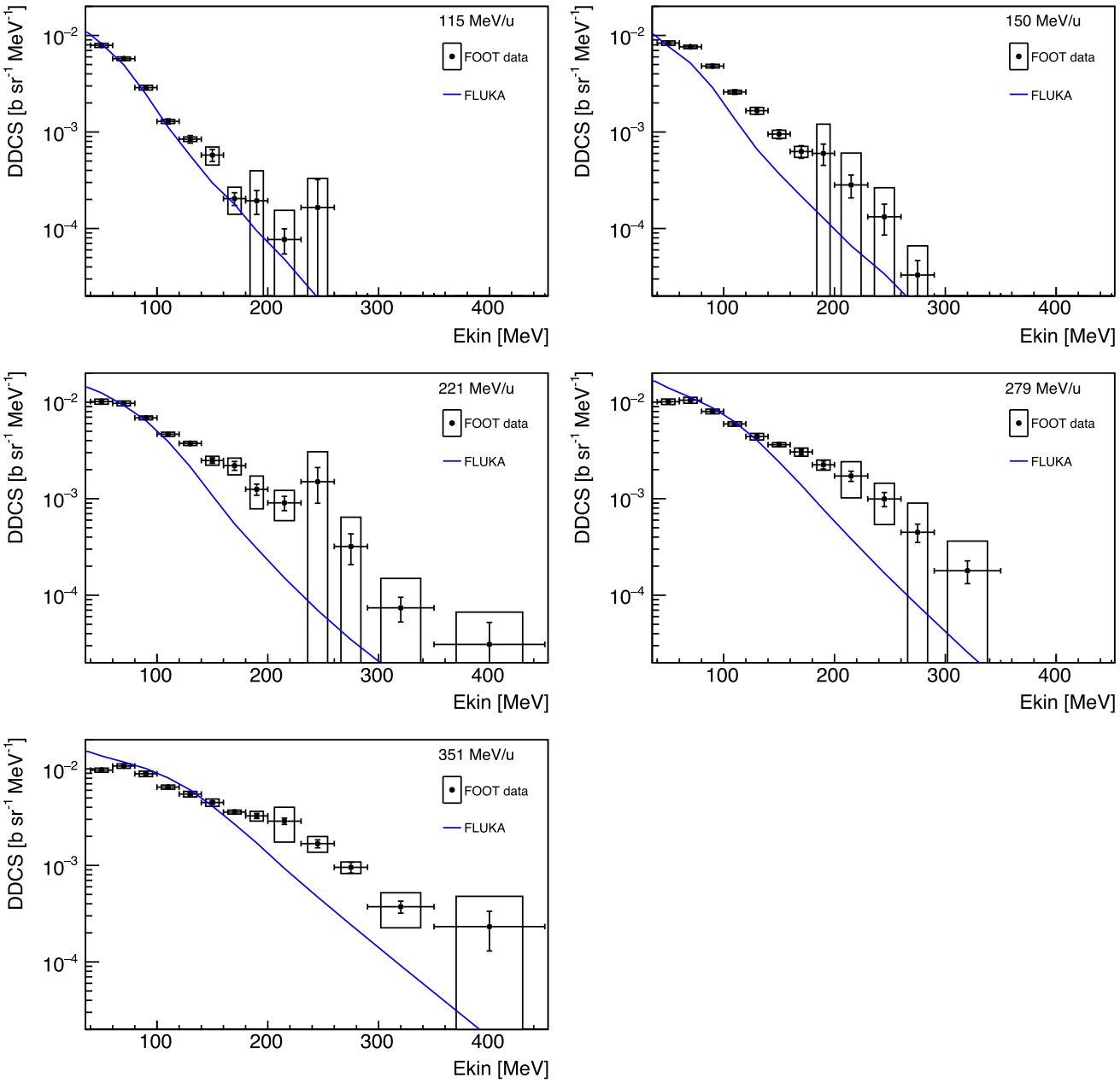

Fig. 10 Double differential cross section as a function of kinetic energy for proton fragments detected at 60°, produced in the nuclear interaction of 115–351 MeV/u carbon ion beam with a PMMA target. The statistical uncertainty (cross) and systematic uncertainty (empty square) on experimental data are shown as separate contributions

an already published dataset [16], refining the efficiency calculation strategy, taking into account the efficiency dependency to the fragment production kinetic energy. Also the calculation of the fragments kinetic energy at production has been improved, applying an unfolding technique to the measured fragment kinetic energy instead of implementing an analytic correction function, as it was done in the previously published results.

In Fig. 13, the comparison of the novel cross sections (red full squares) to the previously published ones [16] (black open circles) is shown for the case of integrated proton fragments cross sections detected at 90° (left) and 60° (right), produced from the interaction of carbon beams with graphite target. For the case of protons detected at 90° a systematic lower shift of new results between 10 and 30% has been found with respect to the old data, while old and new results are in agreement within error bars at 60° detection angle.

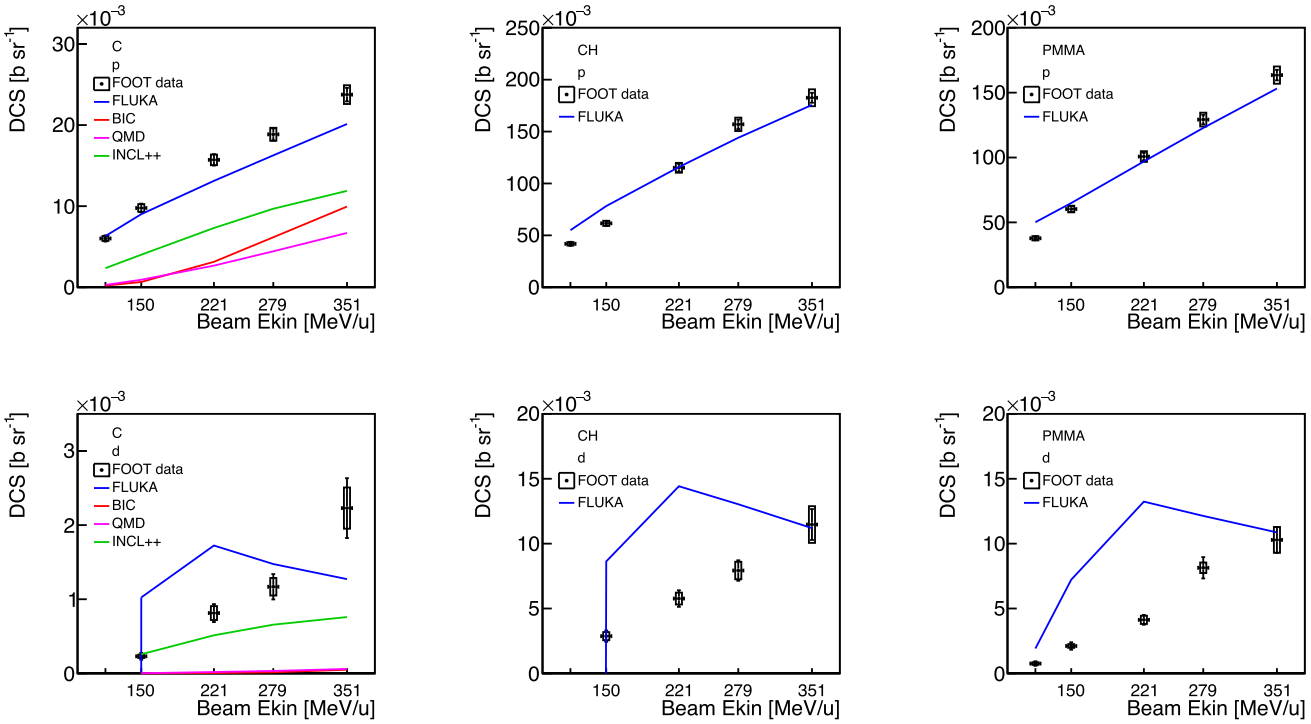

Fig. 11 Energy integrated differential cross section as a function of carbon ion beam kinetic energy for proton (top), deuteron (middle) and triton (bottom) fragments detected at 90°, produced in the nuclear interaction of 115–351 MeV/u carbon ion beam with graphite (C, left), polyvinyl-toluene (CH, middle) and PMMA (right) targets. The integrated energy interval is between E_k = 40–250 MeV/u. Experimental data are shown as black squares, the FLUKA MC prediction is shown as blue line. The statistical uncertainty (cross) and systematic uncertainty (empty square) on experimental data are shown as separate contributions. Cross section for tritons detected at 90° is not reported due to insufficient statistics, as well as deuterons detected at 90° produced by 115 MeV/u ^{12}C ion beam impinging on C and CH targets. For the case of graphite target, the Geant4 models predictions are superimposed

The production of Z = 1 fragments above 60 degrees represents a small fraction of their whole yield coming from the nuclear fragmentation process of ^{12}C projectiles. Using FLUKA, it has been estimated that in C-C collisions at the primary energies considered in this work, the fraction of protons emitted at angles exceeding 60 degrees is about 3% of their total emission in the forward hemisphere. In the case of deuterons and tritons, such a percentage is even a bit lower (2.2–2.8%). In the last decades, significant efforts have been made by developers to improve the reliability of phenomenological models for hadron therapy use, leading to considerable progress. However, it has to be remarked once again that the forward production dominates. The behavior of theory-driven microscopic models of high quality MC codes is generally determined by a limited number of parameters, making it challenging to achieve accurate reproduction of experimental data in the whole phase space. Therefore, the comparison of predictions in the large angle region can be considered a real stress test for these models, and it can be considered as a further added value of the shown results. Our results show that FLUKA provides reasonable predictions for protons in almost the whole explored range. This is instead not the case for deuterons and tritons, with the exception of 115-150 MeV/u primary energy at 60° and of 351 MeV/u primary energy at 90°, although in the latter case, the agreement might just be accidental, given the anomalous behavior as a function of energy. For the reasons above summarized, the presence of discrepancies in this region cannot be considered surprising or alarming. In this respect, it is worthwhile pointing out that in the case of FLUKA, as explained in [34], there is a transition of internal models of nucleus–nucleus interactions around 125 MeV/u, from BME [35] to rQMD [36,37]. The behavior of FLUKA for deuterons and tritons for 150 MeV/u and beyond might suggest possible issues in the rQMD model near its lower energy limit. This has been recently pointed out to the FLUKA developers. It must also be considered that, with respect to deuterons and tritons, the emission of low energy protons may be more heavily affected by later phases of the interaction, such as the pre-equilibrium process. Understanding the deviations between the data and the simulations is part of future research. The comparison with other models from Geant4 has been made for the case of the graphite target. Three different hadronic models have been used: Binary Ion Cascade (BIC) [38], Quan-

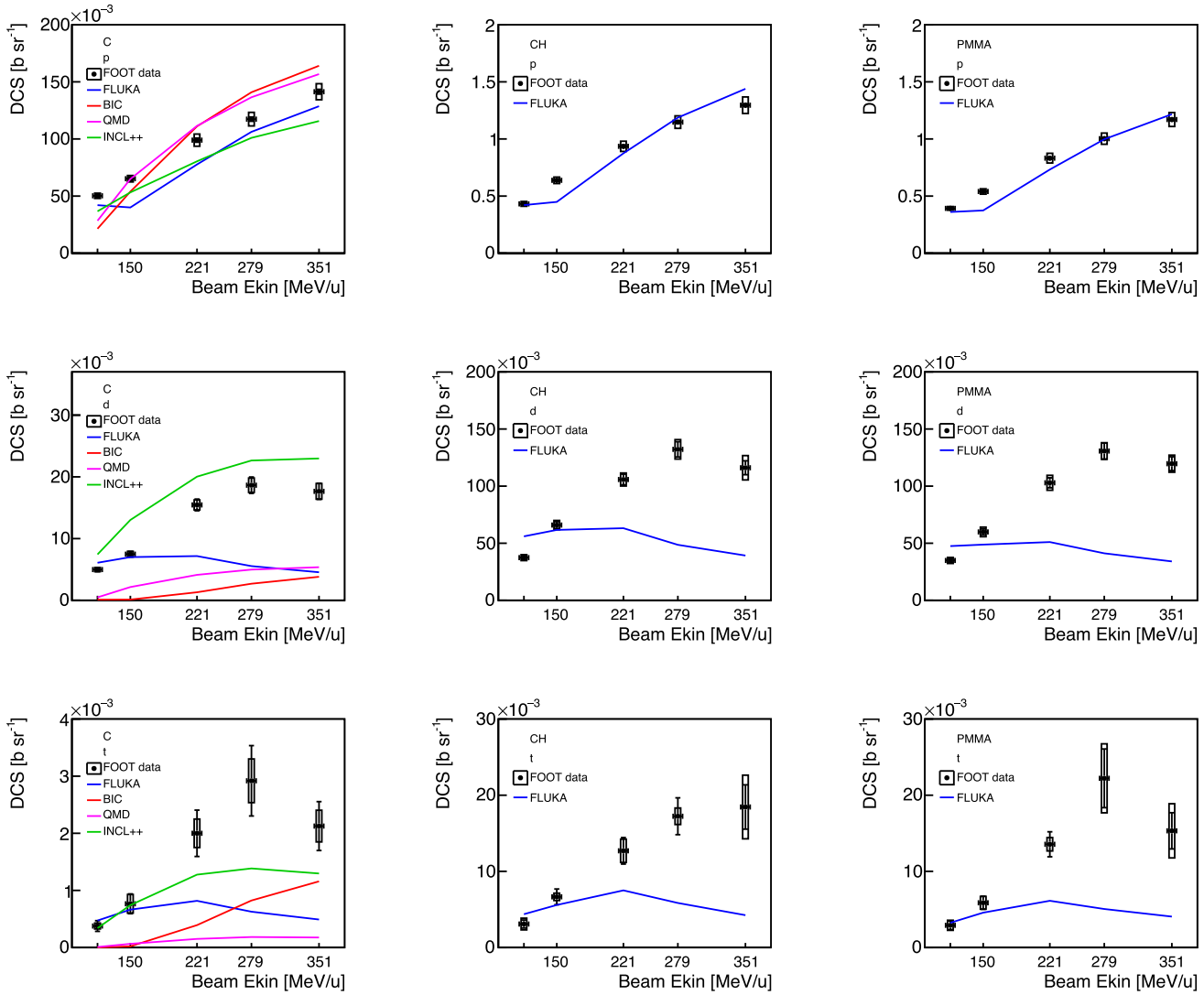

Fig. 12 Energy integrated differential cross section as a function of carbon ion beam kinetic energy for proton (top), deuteron (middle) and triton (bottom) fragments detected at 60°, produced in the nuclear interaction of 115–351 MeV/u carbon ion beam with graphite (C, left), polyvinyl-toluene (CH, middle) and PMMA (right) targets. The integrated energy interval is between E_k = 40– 350 MeV/u. Experimental data are shown as black squares, the FLUKA MC prediction is shown as blue line. The statistical uncertainty (cross) and systematic uncertainty (empty square) on experimental data are shown as separate contributions. For the case of graphite target, the Geant4 models predictions are superimposed

tum Molecular Dynamics (QMD) [39] and Liège Intranuclear Cascade (INCL++) [40]. BIC is a specialized physics library designed to handle ion-ion interactions. It exploits the G4IonPhysics library, using Glauber–Gribov cross sections for all nucleus-nucleus interactions with Precompound/de-excitation for energies below 3 GeV/u. The QMD library, implemented through the G4IonQMDPhysics library, applies a microscopic approach to simulate nuclear collisions and it is often exploited in medical physics applications. Nucleons are simulated as wave packets with a quantum molecular dynamics evolution, which allows to represent nuclear interactions in a more realistic way with respect to simplified models. The INCL++ model simulates the nuclear reactions as a series of independent nucleon-nucleon collisions within the target nucleus. Nucleons are modeled as a free Fermi gas within a static potential well. In the simulated collision of projectile nucleons in a target volume, a quasi-projectile is formed from projectile spectators and non-cascading participants. Then, the quasi-target final state is generated from the full cascade dynamics within the target volume, reproducing a more reliable description of the target remnant. INCL++ typically operates in inverse kinematics approach, better simulating the projectile fragmentation.

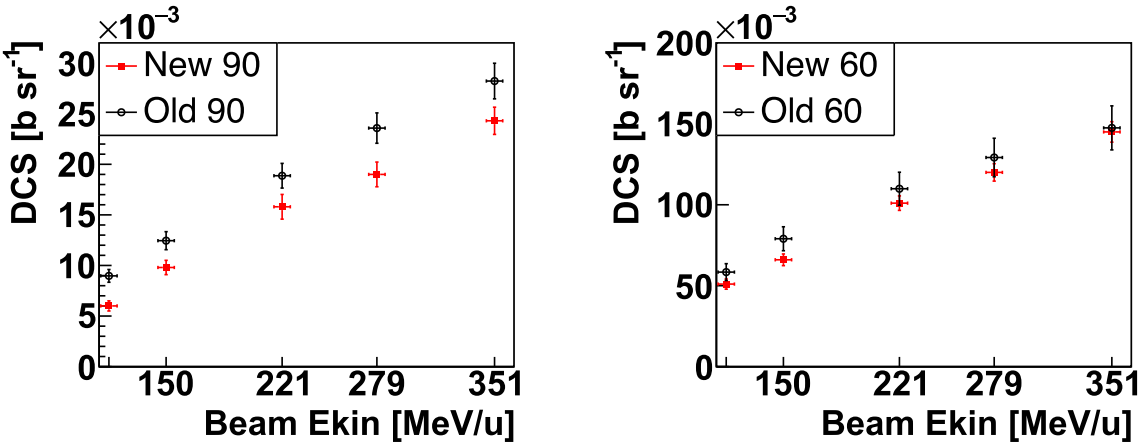

Fig. 13 Comparison of the new (red full squares) and old (black open circles) energy integrated differential cross sections obtained for secondary proton fragments (p) detected at 90° (left) and 60° (right) from the interaction of 115–351 MeV/u ^{12}C ion beam with graphite (C) target

For the case of the double differential cross sections of protons detected at 90°, in Fig. 5, the BIC and QMD Geant4 models are always underestimating the experimental cross sections, while the INCL++ model significantly underestimates the lowest proton energies, below 100 MeV, which are the most populated fragment energies. The same behavior is visible from the proton energy integrated differential cross section, in Fig. 11 (top left). Regarding the double differential cross sections of protons detected at 60°, in Fig. 6, while the BIC and QMD models underestimate significantly the case of 115 MeV/u beam energy, for the other beam energies those models overestimate the lowest, most populated, secondary protons kinetic energy bins, resulting in a slight overestimation of the energy integrated differential cross section for beam energies above 150 MeV/u, visible in Fig. 12 (top left). On the other hand, the INCL++ model better reproduce the double differential experimental cross section behavior at 60°, also with respect to the FLUKA MC. The INCL++ Geant4 model is the one, between the other studied models and MC, that shows the experimental data trend also in the case of deuterons at 90° for the beam energy up to 279 MeV/u (in Fig. 11 – bottom left) and especially at 60° (in Fig. 12 - middle left), with a slight overestimation of the experimental cross sections overall. The case of tritons secondary fragments, shown for the energy integrated differential cross section in the 60° angular configuration, is well reproduced also by INCL++ Geant4 model, as well as FLUKA MC, for the beam energies up to 150 MeV/u, above which the agreement between experimental data and Monte Carlo models is lost in terms of absolute value and trend. Anyway, because of the aforementioned limited number of parameters of theory-driven microscopic models of high quality MC codes, limiting an accurate reproduction of experimental data in the whole phase space, the presence of discrepancies of Monte Carlo predictions with respect to experimental data, for beam energies below the GeV/u and large angle fragments production, cannot be considered surprising or alarming.

From the experimental point of view, it may also be important to investigate potential differences among the Z = 1 isotopes measured at small polar angles. This task could be addressed by the FOOT experiment [17].

Acknowledgements Authors sincerely thank Marco Magi (*Dipartimento di Scienze di Base e Applicate per l'Ingegneria*, Sapienza Università di Roma) for his effort in the construction of mechanical supports for the experimental setup. We are indebted to CNAO particle therapy center for encouraging this measurement, made possible by its support and by the help of the whole CNAO staff. This work has been partially supported by the Tuscany Government, POR FSE 2014 -2020, through the PETRA - INFN-RT2 172800 Project.

Data Availability Statement This manuscript has no associated data. [Author's comment: xxx].

Code Availability Statement This manuscript has no associated code/software. [Author's comment: xxx].

Appendix A. Double differential cross section tables

The double differential cross sections for protons and the energy integrated differential cross sections for protons, deuterons and tritons are here reported for each carbon ion beam energy (115–351 MeV/u) and two detection arms (90°,60°) (see Tables 2, 3, 4, 5, 6, 7, 8, 9, 10, 11, 12, 13, 14, 15, 16, 17, 18, 19, 20, 22,21, 23, 24, 25).

Table 2 Double differential cross section in kinetic energy bins at production (E^p_{kin}) of protons produced by 115 MeV/u ^{12}C ion beam impinging on a C target, detected at 90° (top panel) and 60° (bottom panel). The production cross section from the FLUKA Monte Carlo simulation (*MC*) is listed alongside the experimental cross section (*data*), with the relative statistical and systematic data uncertainties reported as percentage in the last two columns

E^p_{kin} [MeV]	$\frac{d^2\sigma^{MC}}{d\Omega dE_k}$ [b/sr/MeV]	$\frac{d^2\sigma^{data}}{d\Omega dE_k}$ [b/sr/MeV]	Δ^{data}_{stat} [%]	Δ^{data}_{sys} [%]
90°	$\times 10^{-4}$	$\times 10^{-4}$		
40–60	1.79 ± 0.03	$1.9 \pm 0.2 \pm 0.1$	8	7
60–80	0.71 ± 0.02	$0.73 \pm 0.10 \pm 0.04$	13	5
80–100	0.36 ± 0.01	$0.21 \pm 0.04 \pm 0.03$	20	12
100–120	0.173 ± 0.008	$0.082 \pm 0.026 \pm 0.009$	32	11
120–140	0.076 ± 0.005	–	–	–
140–180	0.025 ± 0.002	–	–	–
60°	$\times 10^{-4}$	$\times 10^{-4}$		
40–60	8.96 ± 0.06	$9.1 \pm 0.3 \pm 0.7$	4	8
60–80	5.95 ± 0.05	$7.4 \pm 0.4 \pm 0.3$	5	5
80–100	3.15 ± 0.04	$4.2 \pm 0.3 \pm 0.3$	7	7
100–120	1.45 ± 0.03	$2.0 \pm 0.2 \pm 0.1$	9	6
120–140	0.69 ± 0.02	$1.09 \pm 0.14 \pm 0.10$	13	9
140–160	0.36 ± 0.01	$0.74 \pm 0.15 \pm 0.08$	21	11
160–180	0.196 ± 0.009	$0.37 \pm 0.10 \pm 0.05$	26	13
180–200	0.128 ± 0.008	$0.23 \pm 0.08 \pm 0.07$	35	32
200–230	0.057 ± 0.004	$0.5 \pm 0.5 \pm 0.4$	97	70
230–260	0.021 ± 0.003	–	–	–
260–290	0.008 ± 0.002	–	–	–

Table 3 Double differential cross section in kinetic energy bins at production (E^p_{kin}) of protons produced by 150 MeV/u ^{12}C ion beam impinging on a C target, detected at 90° (top panel) and 60° (bottom panel). The production cross section from the FLUKA Monte Carlo simulation (*MC*) is listed alongside the experimental cross section (*data*), with the relative statistical and systematic data uncertainties reported as percentage in the last two columns

E^p_{kin} [MeV]	$\frac{d^2\sigma^{MC}}{d\Omega dE_k}$ [b/sr/MeV]	$\frac{d^2\sigma^{data}}{d\Omega dE_k}$ [b/sr/MeV]	Δ^{data}_{stat} [%]	Δ^{data}_{sys} [%]
90°	$\times 10^{-4}$	$\times 10^{-4}$		
40–60	2.39 ± 0.03	$3.0 \pm 0.2 \pm 0.1$	8	5
60–80	1.11 ± 0.02	$1.20 \pm 0.13 \pm 0.10$	11	8
80–100	0.51 ± 0.01	$0.42 \pm 0.07 \pm 0.03$	16	8
100–120	0.252 ± 0.010	$0.172 \pm 0.036 \pm 0.009$	21	5
120–140	0.122 ± 0.007	$0.14 \pm 0.06 \pm 0.03$	40	21
140–180	0.049 ± 0.003	–	–	–
180–250	0.0069 ± 0.0009	–	–	–
60°	$\times 10^{-4}$	$\times 10^{-4}$		
40–60	7.52 ± 0.06	$9.9 \pm 0.4 \pm 0.5$	4	6
60–80	5.44 ± 0.05	$9.1 \pm 0.4 \pm 0.4$	5	5
80–100	3.34 ± 0.04	$5.3 \pm 0.3 \pm 0.4$	6	7
100–120	1.69 ± 0.03	$3.2 \pm 0.3 \pm 0.2$	8	5
120–140	0.85 ± 0.02	$2.4 \pm 0.3 \pm 0.6$	12	26
140–160	0.48 ± 0.01	$1.0 \pm 0.1 \pm 0.1$	14	13
160–180	0.27 ± 0.01	$0.7 \pm 0.1 \pm 0.2$	20	31
180–200	0.184 ± 0.009	$0.7 \pm 0.2 \pm 0.2$	30	25
200–230	0.082 ± 0.005	$0.25 \pm 0.08 \pm 0.18$	32	72
230–260	0.043 ± 0.004	$0.16 \pm 0.08 \pm 0.01$	49	9
260–290	0.017 ± 0.002	$0.027 \pm 0.014 \pm 0.006$	51	22
290–350	0.0065 ± 0.0010	$0.04 \pm 0.04 \pm 0.01$	112	27

Table 4 Double differential cross section in kinetic energy bins at production (E^p_{kin}) of protons produced by 221 MeV/u ^{12}C ion beam impinging on a C target, detected at 90° (top panel) and 60° (bottom panel). The production cross section from the FLUKA Monte Carlo simulation (*MC*) is listed alongside the experimental cross section (*data*), with the relative statistical and systematic data uncertainties reported as percentage in the last two columns

E^p_{kin} [MeV]	$\frac{d^2\sigma^{MC}}{d\Omega dE_k}$ [b/sr/MeV]	$\frac{d^2\sigma^{data}}{d\Omega dE_k}$ [b/sr/MeV]	Δ^{data}_{stat} [%]	Δ^{data}_{sys} [%]
90°	$\times 10^{-4}$	$\times 10^{-4}$		
40–60	3.27 ± 0.04	$3.6 \pm 0.2 \pm 0.2$	6	6
60–80	1.65 ± 0.03	$2.1 \pm 0.2 \pm 0.1$	9	7
80–100	0.81 ± 0.02	$1.08 \pm 0.15 \pm 0.08$	14	7
100–120	0.40 ± 0.01	$0.51 \pm 0.09 \pm 0.03$	18	6
120–140	0.215 ± 0.009	$0.25 \pm 0.06 \pm 0.02$	24	9
140–180	0.082 ± 0.004	$0.105 \pm 0.035 \pm 0.007$	33	7
180–250	0.017 ± 0.001	–	–	–
60°	$\times 10^{-4}$	$\times 10^{-4}$		
40–60	12.93 ± 0.08	$10.9 \pm 0.3 \pm 0.7$	3	6
60–80	9.54 ± 0.07	$11.2 \pm 0.4 \pm 0.7$	4	7
80–100	6.72 ± 0.05	$8.2 \pm 0.4 \pm 0.4$	4	5
100–120	4.27 ± 0.04	$5.8 \pm 0.3 \pm 0.4$	6	6
120–140	2.41 ± 0.03	$4.6 \pm 0.3 \pm 0.4$	7	10
140–160	1.32 ± 0.02	$3.2 \pm 0.3 \pm 0.5$	10	16
160–180	0.70 ± 0.02	$2.5 \pm 0.4 \pm 0.4$	14	17
180–200	0.41 ± 0.01	$1.9 \pm 0.4 \pm 1.0$	20	52
200–230	0.189 ± 0.007	$2.0 \pm 0.6 \pm 0.4$	31	19
230–260	0.086 ± 0.005	$0.6 \pm 0.2 \pm 0.3$	33	47
260–290	0.047 ± 0.004	$0.21 \pm 0.08 \pm 0.05$	38	23
290–350	0.017 ± 0.002	$0.17 \pm 0.10 \pm 0.03$	61	17
350–450	0.0028 ± 0.0005	–	–	–

Table 5 Double differential cross section in kinetic energy bins at production (E^p_{kin}) of protons produced by 279 MeV/u ^{12}C ion beam impinging on a C target, detected at 90° (top panel) and 60° (bottom panel). The production cross section from the FLUKA Monte Carlo simulation (*MC*) is listed alongside the experimental cross section (*data*), with the relative statistical and systematic data uncertainties reported as percentage in the last two columns

E^p_{kin} [MeV]	$\frac{d^2\sigma^{MC}}{d\Omega dE_k}$ [b/sr/MeV]	$\frac{d^2\sigma^{data}}{d\Omega dE_k}$ [b/sr/MeV]	Δ^{data}_{stat} [%]	Δ^{data}_{sys} [%]
90°	$\times 10^{-4}$	$\times 10^{-4}$		
40–60	3.99 ± 0.04	$3.8 \pm 0.2 \pm 0.2$	5	4
60–80	2.00 ± 0.03	$2.4 \pm 0.2 \pm 0.1$	8	5
80–100	1.03 ± 0.02	$1.6 \pm 0.2 \pm 0.1$	12	8
100–120	0.54 ± 0.01	$0.88 \pm 0.14 \pm 0.04$	15	5
120–140	0.28 ± 0.01	$0.34 \pm 0.06 \pm 0.03$	18	9
140–180	0.111 ± 0.005	$0.32 \pm 0.11 \pm 0.02$	34	7
180–250	0.020 ± 0.001	$0.06 \pm 0.04 \pm 0.10$	62	177
60°	$\times 10^{-4}$	$\times 10^{-4}$		
40–60	14.77 ± 0.08	$10.7 \pm 0.3 \pm 0.7$	3	6
60–80	11.65 ± 0.07	$11.3 \pm 0.4 \pm 0.5$	3	5
80–100	8.98 ± 0.06	$8.8 \pm 0.3 \pm 0.5$	4	5
100–120	6.50 ± 0.05	$6.9 \pm 0.3 \pm 0.4$	4	5
120–140	4.44 ± 0.04	$6.1 \pm 0.3 \pm 0.3$	6	5
140–160	2.76 ± 0.04	$4.3 \pm 0.3 \pm 0.4$	7	10
160–180	1.66 ± 0.03	$3.4 \pm 0.3 \pm 0.6$	9	17
180–200	0.99 ± 0.02	$2.6 \pm 0.3 \pm 1.0$	12	39
200–230	0.51 ± 0.01	$2.7 \pm 0.5 \pm 1.3$	17	50
230–260	0.234 ± 0.008	$1.5 \pm 0.3 \pm 1.0$	23	70
260–290	0.105 ± 0.006	$1.3 \pm 0.5 \pm 0.7$	41	55

Table 5 continued

E^p_{kin} [MeV]	$\frac{d^2\sigma^{MC}}{d\Omega dE_k}$ [b/sr/MeV]	$\frac{d^2\sigma^{data}}{d\Omega dE_k}$ [b/sr/MeV]	Δ^{data}_{stat} [%]	Δ^{data}_{sys} [%]
290–350	0.033 ± 0.002	$0.4 \pm 0.1 \pm 0.2$	37	51
350–450	0.0053 ± 0.0007	$0.09 \pm 0.08 \pm 0.04$	93	48

Table 6 Double differential cross section in kinetic energy bins at production (E^p_{kin}) of protons produced by 351 MeV/u ^{12}C ion beam impinging on a C target, detected at 90° (top panel) and 60° (bottom panel). The production cross section from the FLUKA Monte Carlo simulation (*MC*) is listed alongside the experimental cross section (*data*), with the relative statistical and systematic data uncertainties reported as percentage in the last two columns

E^p_{kin} [MeV]	$\frac{d^2\sigma^{MC}}{d\Omega dE_k}$ [b/sr/MeV]	$\frac{d^2\sigma^{data}}{d\Omega dE_k}$ [b/sr/MeV]	Δ^{data}_{stat} [%]	Δ^{data}_{sys} [%]
90°	$\times 10^{-4}$	$\times 10^{-4}$		
40–60	4.49 ± 0.04	$4.4 \pm 0.2 \pm 0.3$	5	6
60–80	2.44 ± 0.03	$3.3 \pm 0.2 \pm 0.2$	7	5
80–100	1.42 ± 0.02	$1.7 \pm 0.2 \pm 0.1$	9	8
100–120	0.77 ± 0.02	$1.1 \pm 0.1 \pm 0.2$	13	19
120–140	0.45 ± 0.01	$0.66 \pm 0.11 \pm 0.09$	16	14
140–180	0.185 ± 0.006	$0.34 \pm 0.07 \pm 0.03$	19	7
180–250	0.036 ± 0.002	$0.08 \pm 0.02 \pm 0.04$	32	57
250–350	0.0027 ± 0.0005	–	–	–
60°	$\times 10^{-4}$	$\times 10^{-4}$		
40–60	14.38 ± 0.08	$11.0 \pm 0.3 \pm 0.5$	3	5
60–80	12.11 ± 0.07	$11.6 \pm 0.4 \pm 0.6$	3	5
80–100	10.08 ± 0.07	$10.2 \pm 0.4 \pm 0.5$	4	5
100–120	8.17 ± 0.06	$7.7 \pm 0.3 \pm 0.4$	4	5
120–140	6.35 ± 0.05	$6.2 \pm 0.3 \pm 0.6$	4	10
140–160	4.54 ± 0.04	$5.5 \pm 0.3 \pm 0.5$	6	8
160–180	3.09 ± 0.04	$4.8 \pm 0.3 \pm 0.2$	7	5
180–200	2.08 ± 0.03	$5.4 \pm 0.5 \pm 1.5$	10	27
200–230	1.20 ± 0.02	$4.2 \pm 0.5 \pm 1.2$	11	29
230–260	0.60 ± 0.01	$3.2 \pm 0.6 \pm 1.4$	17	44
260–290	0.317 ± 0.010	$1.6 \pm 0.3 \pm 0.6$	20	38
290–350	0.118 ± 0.004	$0.7 \pm 0.1 \pm 0.3$	20	38
350–450	0.021 ± 0.001	$0.3 \pm 0.2 \pm 0.4$	68	118
450–650	0.0012 ± 0.0002	–	–	–

Table 7 Energy integrated differential cross section of protons produced by ^{12}C ion beam of kinetic energy (E^C_{kin}) ranging from 115 MeV/u to 351 MeV/u impinging on a C target. Protons are detected at 90° (top panel) and 60° (bottom panel). The production cross section from the FLUKA Monte Carlo simulation (*MC*) is listed alongside the experimental cross section (*data*), with the relative statistical and systematic data uncertainties reported as percentage in the last two columns

E^C_{kin} [MeV/u]	$\frac{d\sigma^{MC}}{d\Omega}$ [b/sr]	$\frac{d\sigma^{data}}{d\Omega}$ [b/sr]	Δ^{data}_{stat} [%]	Δ^{data}_{sys} [%]
90°	$\times 10^{-3}$	$\times 10^{-3}$		
115	6.31 ± 0.07	$6.0 \pm 0.4 \pm 0.3$	6	5
150	9.01 ± 0.08	$9.8 \pm 0.5 \pm 0.5$	5	5
221	13.1 ± 0.1	$15.7 \pm 0.7 \pm 0.7$	4	4
279	16.3 ± 0.1	$18.9 \pm 0.7 \pm 0.8$	4	4
351	20.1 ± 0.1	$23.8 \pm 0.8 \pm 1.2$	4	5
60°	$\times 10^{-2}$	$\times 10^{-2}$		
115	4.20 ± 0.02	$5.0 \pm 0.1 \pm 0.2$	3	5
150	4.00 ± 0.02	$6.5 \pm 0.2 \pm 0.3$	2	4
221	7.77 ± 0.03	$9.9 \pm 0.2 \pm 0.5$	2	5
279	10.62 ± 0.03	$11.7 \pm 0.2 \pm 0.6$	2	5
351	12.87 ± 0.03	$14.1 \pm 0.2 \pm 0.7$	1	5

Table 8 Energy integrated differential cross section of deuterons produced by ^{12}C ion beam of kinetic energy (E^C_{kin}) ranging from 115 MeV/u to 351 MeV/u impinging on a C target. Deuterons are detected at 90° (top panel) and 60° (bottom panel). The production cross section from the FLUKA Monte Carlo simulation (*MC*) is listed alongside the experimental cross section (*data*), with the relative statistical and systematic data uncertainties reported as percentage in the last two columns. Cross section of 115 MeV/u ^{12}C ion beam impinging on a C target for deuterons detected at 90° is not reported due to insufficient statistics

E^C_{kin} [MeV/u]	$\frac{d\sigma^{MC}}{d\Omega}$ [b/sr]	$\frac{d\sigma^{data}}{d\Omega}$ [b/sr]	Δ^{data}_{stat} [%]	Δ^{data}_{sys} [%]
90°	$\times 10^{-3}$	$\times 10^{-3}$		
150	1.02 ± 0.03	$0.23 \pm 0.05 \pm 0.02$	20	10
221	1.72 ± 0.04	$0.81 \pm 0.12 \pm 0.09$	15	12
279	1.47 ± 0.03	$1.2 \pm 0.2 \pm 0.1$	15	10
351	1.27 ± 0.03	$2.2 \pm 0.4 \pm 0.3$	18	12
60°	$\times 10^{-2}$	$\times 10^{-2}$		
115	0.609 ± 0.007	$0.50 \pm 0.03 \pm 0.03$	7	7
150	0.700 ± 0.008	$0.75 \pm 0.04 \pm 0.05$	6	6
221	0.717 ± 0.008	$1.55 \pm 0.09 \pm 0.08$	6	5
279	0.555 ± 0.007	$1.9 \pm 0.1 \pm 0.1$	7	6
351	0.455 ± 0.006	$1.8 \pm 0.1 \pm 0.1$	7	7

Table 9 Energy integrated differential cross section of tritons produced by ^{12}C ion beam of kinetic energy (E^C_{kin}) ranging from 115 MeV/u to 351 MeV/u impinging on a C target. Tritons are detected at 60°. The production cross section from the FLUKA Monte Carlo simulation (*MC*) is listed alongside the experimental cross section (*data*), with the relative statistical and systematic data uncertainties reported as percentage in the last two columns. Cross section for tritons detected at 90° is not reported due to insufficient statistics

E^C_{kin} [MeV/u]	$\frac{d\sigma^{MC}}{d\Omega}$ [b/sr]	$\frac{d\sigma^{data}}{d\Omega}$ [b/sr]	Δ^{data}_{stat} [%]	Δ^{data}_{sys} [%]
60°	$\times 10^{-3}$	$\times 10^{-3}$		
115	0.47 ± 0.02	$0.38 \pm 0.09 \pm 0.05$	25	14
150	0.66 ± 0.02	$0.8 \pm 0.2 \pm 0.2$	23	21
221	0.82 ± 0.03	$2.0 \pm 0.4 \pm 0.2$	20	12
279	0.63 ± 0.02	$2.9 \pm 0.6 \pm 0.4$	21	13
351	0.49 ± 0.02	$2.1 \pm 0.4 \pm 0.3$	20	13

Table 10 Double differential cross section in kinetic energy bins at production (E^p_{kin}) of protons produced by 115 MeV/u ^{12}C ion beam impinging on a CH target, detected at 90° (top panel) and 60° (bottom panel). The production cross section from the FLUKA Monte Carlo simulation (*MC*) is listed alongside the experimental cross section (*data*), with the relative statistical and systematic data uncertainties reported as percentage in the last two columns

E^p_{kin} [MeV]	$\frac{d^2\sigma^{MC}}{d\Omega dE_k}$ [b/sr/MeV]	$\frac{d^2\sigma^{data}}{d\Omega dE_k}$ [b/sr/MeV]	Δ^{data}_{stat} [%]	Δ^{data}_{sys} [%]
90°	$\times 10^{-5}$	$\times 10^{-5}$		
40–60	154 ± 2	$138 \pm 8 \pm 6$	6	4
60–80	64 ± 1	$49 \pm 5 \pm 2$	10	4
80–100	30.6 ± 0.7	$17 \pm 2 \pm 1$	14	7
100–120	14.6 ± 0.5	$5.3 \pm 1.0 \pm 0.2$	19	4
120–140	6.8 ± 0.3	–	–	–
140–180	2.2 ± 0.1	–	–	–
180–250	0.23 ± 0.03	–	–	–
60°	$\times 10^{-5}$	$\times 10^{-5}$		
40–60	979 ± 4	$857 \pm 21 \pm 54$	2	6

Table 10 continued

E^p_{kin} [MeV]	$\frac{d^2\sigma^{MC}}{d\Omega dE_k}$ [b/sr/MeV]	$\frac{d^2\sigma^{data}}{d\Omega dE_k}$ [b/sr/MeV]	Δ^{data}_{stat} [%]	Δ^{data}_{sys} [%]
60–80	576 ± 3	$671 \pm 21 \pm 33$	3	5
80–100	289 ± 2	$320 \pm 14 \pm 18$	4	5
100–120	129 ± 2	$137 \pm 9 \pm 6$	6	4
120–140	61 ± 1	$91 \pm 9 \pm 10$	10	11
140–160	32.6 ± 0.8	$46 \pm 6 \pm 8$	13	18
160–180	17.4 ± 0.6	$20 \pm 3 \pm 6$	17	29
180–200	10.5 ± 0.5	$15 \pm 4 \pm 4$	27	26
200–230	5.1 ± 0.3	$7 \pm 2 \pm 14$	29	212
230–260	1.6 ± 0.1	$4 \pm 2 \pm 2$	57	53
260–290	0.71 ± 0.10	–	–	–

Table 11 Double differential cross section in kinetic energy bins at production (E^p_{kin}) of protons produced by 150 MeV/u ^{12}C ion beam impinging on a CH target, detected at 90° (top panel) and 60° (bottom panel). The production cross section from the FLUKA Monte Carlo simulation (*MC*) is listed alongside the experimental cross section (*data*), with the relative statistical and systematic data uncertainties reported as percentage in the last two columns

E^p_{kin} [MeV]	$\frac{d^2\sigma^{MC}}{d\Omega dE_k}$ [b/sr/MeV]	$\frac{d^2\sigma^{data}}{d\Omega dE_k}$ [b/sr/MeV]	Δ^{data}_{stat} [%]	Δ^{data}_{sys} [%]
90°	$\times 10^{-5}$	$\times 10^{-5}$		
40–60	209 ± 2	$176 \pm 9 \pm 7$	5	4
60–80	95 ± 1	$83 \pm 7 \pm 6$	8	7
80–100	45.9 ± 0.9	$31 \pm 3 \pm 4$	11	14
100–120	22.1 ± 0.6	$11 \pm 2 \pm 1$	15	10
120–140	10.4 ± 0.4	$3.7 \pm 0.8 \pm 0.4$	23	12
140–180	3.7 ± 0.2	–	–	–
180–250	0.57 ± 0.05	–	–	–
60°	$\times 10^{-5}$	$\times 10^{-5}$		
40–60	934 ± 4	$1059 \pm 27 \pm 53$	3	5
60–80	620 ± 4	$843 \pm 25 \pm 39$	3	5
80–100	349 ± 3	$556 \pm 23 \pm 28$	4	5
100–120	164 ± 2	$304 \pm 18 \pm 15$	6	5
120–140	76 ± 1	$181 \pm 15 \pm 8$	8	5
140–160	42.5 ± 0.9	$93 \pm 10 \pm 14$	11	15
160–180	24.2 ± 0.7	$79 \pm 14 \pm 25$	17	32
180–200	14.3 ± 0.5	$40 \pm 9 \pm 18$	21	44
200–230	7.9 ± 0.3	$27 \pm 7 \pm 15$	26	55
230–260	3.5 ± 0.2	$21 \pm 10 \pm 9$	50	45
260–290	1.7 ± 0.2	$5 \pm 2 \pm 2$	49	41
290–350	0.45 ± 0.05	$4 \pm 4 \pm 2$	113	42

Table 12 Double differential cross section in kinetic energy bins at production (E^p_{kin}) of protons produced by 221 MeV/u ^{12}C ion beam impinging on a CH target, detected at 90° (top panel) and 60° (bottom panel). The production cross section from the FLUKA Monte Carlo simulation (*MC*) is listed alongside the experimental cross section (*data*), with the relative statistical and systematic data uncertainties reported as percentage in the last two columns

E^p_{kin} [MeV]	$\frac{d^2\sigma^{MC}}{d\Omega dE_k}$ [b/sr/MeV]	$\frac{d^2\sigma^{data}}{d\Omega dE_k}$ [b/sr/MeV]	Δ^{data}_{stat} [%]	Δ^{data}_{sys} [%]
90°	$\times 10^{-5}$	$\times 10^{-5}$		
40–60	289 ± 2	$297 \pm 15 \pm 19$	5	6
60–80	145 ± 2	$128 \pm 8 \pm 13$	6	10
80–100	71 ± 1	$78 \pm 8 \pm 11$	10	14
100–120	34.7 ± 0.8	$41 \pm 5 \pm 6$	13	14
120–140	18.9 ± 0.6	$21 \pm 4 \pm 4$	21	19
140–180	7.4 ± 0.3	$6 \pm 1 \pm 1$	21	21
180–250	1.54 ± 0.09	$1.1 \pm 0.4 \pm 0.5$	32	45
250–350	0.17 ± 0.03	–	–	–
60°	$\times 10^{-5}$	$\times 10^{-5}$		
40–60	1492 ± 6	$1127 \pm 24 \pm 59$	2	5
60–80	1111 ± 5	$1100 \pm 26 \pm 57$	2	5
80–100	766 ± 4	$808 \pm 23 \pm 37$	3	5
100–120	472 ± 3	$534 \pm 20 \pm 24$	4	5
120–140	252 ± 2	$371 \pm 18 \pm 16$	5	4
140–160	129 ± 2	$262 \pm 18 \pm 22$	7	9
160–180	64 ± 1	$189 \pm 19 \pm 35$	10	18
180–200	35.2 ± 0.9	$159 \pm 25 \pm 22$	16	14
200–230	18.4 ± 0.5	$125 \pm 24 \pm 42$	19	33
230–260	8.7 ± 0.4	$69 \pm 20 \pm 30$	29	44
260–290	3.9 ± 0.2	$29 \pm 11 \pm 8$	38	27
290–350	1.4 ± 0.1	$6 \pm 2 \pm 3$	31	52
350–450	0.32 ± 0.04	–	–	–

Table 13 Double differential cross section in kinetic energy bins at production (E^p_{kin}) of protons produced by 279 MeV/u ^{12}C ion beam impinging on a CH target, detected at 90° (top panel) and 60° (bottom panel). The production cross section from the FLUKA Monte Carlo simulation (*MC*) is listed alongside the experimental cross section (*data*), with the relative statistical and systematic data uncertainties reported as percentage in the last two columns

E^p_{kin} [MeV]	$\frac{d^2\sigma^{MC}}{d\Omega dE_k}$ [b/sr/MeV]	$\frac{d^2\sigma^{data}}{d\Omega dE_k}$ [b/sr/MeV]	Δ^{data}_{stat} [%]	Δ^{data}_{sys} [%]
90°	$\times 10^{-5}$	$\times 10^{-5}$		
40–60	351 ± 2	$330 \pm 14 \pm 14$	4	4
60–80	179 ± 2	$208 \pm 12 \pm 9$	6	4
80–100	93 ± 1	$115 \pm 9 \pm 7$	8	6
100–120	48.4 ± 0.9	$68 \pm 7 \pm 8$	11	12
120–140	23.8 ± 0.6	$27 \pm 4 \pm 6$	15	22
140–180	9.4 ± 0.3	$18 \pm 4 \pm 3$	20	14
180–250	1.64 ± 0.09	$3.3 \pm 1.3 \pm 0.7$	38	20
250–350	0.16 ± 0.02	–	–	–
60°	$\times 10^{-5}$	$\times 10^{-5}$		
40–60	1662 ± 6	$1142 \pm 23 \pm 63$	2	5
60–80	1333 ± 5	$1195 \pm 25 \pm 69$	2	6
80–100	1042 ± 5	$938 \pm 23 \pm 50$	2	5
100 - 120	744 ± 4	$686 \pm 20 \pm 32$	3	5
120–140	484 ± 3	$513 \pm 18 \pm 43$	3	8
140–160	286 ± 2	$387 \pm 18 \pm 37$	5	9
160–180	169 ± 2	$303 \pm 19 \pm 24$	6	8

Table 13 continued

E^p_{kin} [MeV]	$\frac{d^2\sigma^{MC}}{d\Omega dE_k}$ [b/sr/MeV]	$\frac{d^2\sigma^{data}}{d\Omega dE_k}$ [b/sr/MeV]	Δ^{data}_{stat} [%]	Δ^{data}_{sys} [%]
180–200	92 ± 1	$293 \pm 29 \pm 92$	10	31
200–230	46.4 ± 0.8	$222 \pm 26 \pm 100$	12	45
230–260	20.1 ± 0.5	$118 \pm 20 \pm 45$	17	38
260–290	8.9 ± 0.3	$72 \pm 20 \pm 27$	28	38
290–350	3.0 ± 0.1	$16 \pm 4 \pm 6$	24	39
350–450	0.37 ± 0.04	$4 \pm 3 \pm 3$	67	64

Table 14 Double differential cross section in kinetic energy bins at production (E^p_{kin}) of protons produced by 351 MeV/u ^{12}C ion beam impinging on a CH target, detected at 90° (top panel) and 60° (bottom panel). The production cross section from the FLUKA Monte Carlo simulation (*MC*) is listed alongside the experimental cross section (*data*), with the relative statistical and systematic data uncertainties reported as percentage in the last two columns

E^p_{kin} [MeV]	$\frac{d^2\sigma^{MC}}{d\Omega dE_k}$ [b/sr/MeV]	$\frac{d^2\sigma^{data}}{d\Omega dE_k}$ [b/sr/MeV]	Δ^{data}_{stat} [%]	Δ^{data}_{sys} [%]
90°	$\times 10^{-5}$	$\times 10^{-5}$		
40–60	391 ± 3	$355 \pm 14 \pm 21$	4	6
60–80	213 ± 2	$222 \pm 12 \pm 15$	5	7
80–100	124 ± 1	$145 \pm 10 \pm 8$	7	6
100–120	71 ± 1	$78 \pm 7 \pm 14$	9	18
120–140	38.2 ± 0.8	$56 \pm 8 \pm 6$	14	10
140–180	15.6 ± 0.4	$21 \pm 3 \pm 2$	13	8
180–250	3.1 ± 0.1	$8 \pm 2 \pm 1$	28	14
250–350	0.31 ± 0.03	$0.39 \pm 0.17 \pm 0.08$	44	21
60°	$\times 10^{-5}$	$\times 10^{-5}$		
40–60	1603 ± 6	$1030 \pm 20 \pm 76$	2	7
60–80	1395 ± 5	$1269 \pm 27 \pm 81$	2	6
80–100	1190 ± 5	$986 \pm 22 \pm 51$	2	5
100–120	955 ± 4	$693 \pm 17 \pm 38$	2	5
120–140	716 ± 4	$612 \pm 18 \pm 44$	3	7
140–160	487 ± 3	$526 \pm 19 \pm 28$	4	5
160–180	319 ± 3	$403 \pm 18 \pm 47$	5	12
180–200	203 ± 2	$324 \pm 20 \pm 51$	6	16
200–230	112 ± 1	$340 \pm 26 \pm 163$	8	48
230–260	55.8 ± 0.9	$211 \pm 23 \pm 91$	11	43
260–290	28.3 ± 0.6	$82 \pm 10 \pm 19$	12	23
290–350	10.3 ± 0.3	$47 \pm 7 \pm 11$	14	24
350–450	1.95 ± 0.09	$29 \pm 13 \pm 5$	44	16
450–650	0.08 ± 0.01	–	–	–

Table 15 Energy integrated differential cross section of protons produced by ^{12}C ion beam of kinetic energy (E^C_{kin}) ranging from 115 MeV/u to 351 MeV/u impinging on a CH target. Protons are detected at 90° (top panel) and 60° (bottom panel). The production cross section from the FLUKA Monte Carlo simulation (*MC*) is listed alongside the experimental cross section (*data*), with the relative statistical and systematic data uncertainties reported as percentage in the last two columns

E^C_{kin} [MeV/u]	$\frac{d\sigma^{MC}}{d\Omega}$ [b/sr]	$\frac{d\sigma^{data}}{d\Omega}$ [b/sr]	Δ^{data}_{stat} [%]	Δ^{data}_{sys} [%]
90°	$\times 10^{-3}$	$\times 10^{-3}$		
115	55.0 ± 0.4	$42 \pm 2 \pm 2$	5	4
150	78.2 ± 0.5	$62 \pm 2 \pm 2$	4	4
221	115.8 ± 0.7	$115 \pm 4 \pm 5$	3	4
279	144.0 ± 0.7	$157 \pm 5 \pm 6$	3	4
351	175.7 ± 0.8	$183 \pm 5 \pm 8$	3	4
60°	$\times 10^{-2}$	$\times 10^{-2}$		
115	42.1 ± 0.1	$43.2 \pm 0.7 \pm 2.1$	2	5
150	44.9 ± 0.1	$64 \pm 1 \pm 3$	2	4
221	87.4 ± 0.2	$94 \pm 1 \pm 4$	1	5
279	118.7 ± 0.2	$115 \pm 1 \pm 5$	1	5
351	143.9 ± 0.2	$130 \pm 1 \pm 7$	1	6

Table 16 Energy integrated differential cross section of deuterons produced by ^{12}C ion beam of kinetic energy (E^C_{kin}) ranging from 115 MeV/u to 351 MeV/u impinging on a CH target. Deuterons are detected at 90° (top panel) and 60° (bottom panel). The production cross section from the FLUKA Monte Carlo simulation (*MC*) is listed alongside the experimental cross section (*data*), with the relative statistical and systematic data uncertainties reported as percentage in the last two columns. Cross section of 115 MeV/u ^{12}C ion beam impinging on a CH target for deuterons detected at 90° is not reported due to insufficient statistics

E^C_{kin} [MeV/u]	$\frac{d\sigma^{MC}}{d\Omega}$ [b/sr]	$\frac{d\sigma^{data}}{d\Omega}$ [b/sr]	Δ^{data}_{stat} [%]	Δ^{data}_{sys} [%]
90°	$\times 10^{-4}$	$\times 10^{-4}$		
150	86 ± 2	$29 \pm 4 \pm 3$	15	11
221	144 ± 2	$58 \pm 6 \pm 5$	11	8
279	130 ± 2	$79 \pm 8 \pm 7$	10	9
351	112 ± 2	$115 \pm 12 \pm 14$	10	12
60°	$\times 10^{-3}$	$\times 10^{-3}$		
115	56.0 ± 0.5	$37 \pm 2 \pm 3$	5	7
150	61.7 ± 0.5	$66 \pm 3 \pm 4$	4	6
221	63.2 ± 0.5	$106 \pm 5 \pm 6$	4	5
279	48.6 ± 0.4	$132 \pm 7 \pm 9$	5	6
351	39.2 ± 0.4	$116 \pm 6 \pm 11$	5	9

Table 17 Energy integrated differential cross section of tritons produced by ^{12}C ion beam of kinetic energy (E^C_{kin}) ranging from 115 MeV/u to 351 MeV/u impinging on a CH target. Tritons are detected at 60°. The production cross section from the FLUKA Monte Carlo simulation (*MC*) is listed alongside the experimental cross section (*data*), with the relative statistical and systematic data uncertainties reported as percentage in the last two columns. Cross section for tritons detected at 90° is not reported due to insufficient statistics

E^C_{kin} [MeV/u]	$\frac{d\sigma^{MC}}{d\Omega}$ [b/sr]	$\frac{d\sigma^{data}}{d\Omega}$ [b/sr]	Δ^{data}_{stat} [%]	Δ^{data}_{sys} [%]
60°	$\times 10^{-4}$	$\times 10^{-4}$		
115	44 ± 1	$31 \pm 5 \pm 8$	17	25
150	56 ± 1	$67 \pm 10 \pm 5$	15	7
221	75 ± 2	$127 \pm 17 \pm 15$	14	12
279	58 ± 2	$172 \pm 24 \pm 11$	14	6
351	42 ± 1	$185 \pm 29 \pm 42$	16	23

Table 18 Double differential cross section in kinetic energy bins at production (E^p_{kin}) of protons produced by 115 MeV/u ^{12}C ion beam impinging on a PMMA target, detected at 90° (top panel) and 60° (bottom panel). The production cross section from the FLUKA Monte Carlo simulation (*MC*) is listed alongside the experimental cross section (*data*), with the relative statistical and systematic data uncertainties reported as percentage in the last two columns

E^p_{kin} [MeV]	$\frac{d^2\sigma^{MC}}{d\Omega dE_k}$ [b/sr/MeV]	$\frac{d^2\sigma^{data}}{d\Omega dE_k}$ [b/sr/MeV]	Δ^{data}_{stat} [%]	Δ^{data}_{sys} [%]
90°	$\times 10^{-4}$	$\times 10^{-4}$		
40–60	13.4 ± 0.1	$12.0 \pm 0.7 \pm 0.7$	5	6
60–80	5.76 ± 0.09	$4.5 \pm 0.4 \pm 0.3$	9	7
80–100	3.01 ± 0.06	$1.48 \pm 0.20 \pm 0.06$	13	4
100–120	1.48 ± 0.04	$0.46 \pm 0.08 \pm 0.08$	18	17
120–140	0.77 ± 0.03	–	–	–
140–180	0.26 ± 0.01	–	–	–
180–250	0.046 ± 0.004	–	–	–
60°	$\times 10^{-4}$	$\times 10^{-4}$		
40–60	82.0 ± 0.3	$79 \pm 2 \pm 4$	2	5
60–80	49.8 ± 0.3	$57 \pm 2 \pm 2$	3	4
80–100	24.7 ± 0.2	$29 \pm 1 \pm 2$	4	6
100–120	11.2 ± 0.1	$12.9 \pm 0.8 \pm 0.6$	6	5
120–140	5.69 ± 0.09	$8.4 \pm 0.8 \pm 0.5$	9	5
140–160	2.97 ± 0.07	$5.8 \pm 0.8 \pm 1.2$	14	21
160–180	1.78 ± 0.05	$2.0 \pm 0.3 \pm 0.6$	15	31
180–200	0.95 ± 0.04	$1.9 \pm 0.5 \pm 0.7$	28	36
200–230	0.48 ± 0.02	$0.8 \pm 0.2 \pm 0.2$	29	22
230–260	0.19 ± 0.01	$1.7 \pm 1.6 \pm 0.3$	95	21
260–290	0.078 ± 0.009	–	–	–
290–350	0.026 ± 0.004	–	–	–

Table 19 Double differential cross section in kinetic energy bins at production (E^p_{kin}) of protons produced by 150 MeV/u ^{12}C ion beam impinging on a PMMA target, detected at 90° (top panel) and 60° (bottom panel). The production cross section from the FLUKA Monte Carlo simulation (*MC*) is listed alongside the experimental cross section (*data*), with the relative statistical and systematic data uncertainties reported as percentage in the last two columns

E^p_{kin} [MeV]	$\frac{d^2\sigma^{MC}}{d\Omega dE_k}$ [b/sr/MeV]	$\frac{d^2\sigma^{data}}{d\Omega dE_k}$ [b/sr/MeV]	Δ^{data}_{stat} [%]	Δ^{data}_{sys} [%]
90°	$\times 10^{-4}$	$\times 10^{-4}$		
40–60	17.3 ± 0.1	$17.0 \pm 0.8 \pm 1.2$	5	7
60–80	7.9 ± 0.1	$7.9 \pm 0.6 \pm 0.7$	8	9
80–100	3.77 ± 0.07	$2.8 \pm 0.3 \pm 0.1$	10	5
100–120	1.82 ± 0.05	$1.5 \pm 0.3 \pm 0.4$	17	24
120–140	0.84 ± 0.03	$0.41 \pm 0.09 \pm 0.10$	22	24
140–180	0.32 ± 0.01	$0.13 \pm 0.03 \pm 0.03$	27	27
180–250	0.059 ± 0.005	–	–	–
60°	$\times 10^{-4}$	$\times 10^{-4}$		
40–60	77.2 ± 0.3	$83 \pm 2 \pm 4$	2	5
60–80	51.8 ± 0.3	$76 \pm 2 \pm 3$	3	4
80–100	28.8 ± 0.2	$48 \pm 2 \pm 2$	4	4
100–120	13.6 ± 0.1	$26 \pm 1 \pm 1$	5	4
120–140	6.63 ± 0.10	$17 \pm 1 \pm 1$	8	8
140–160	3.70 ± 0.07	$9.5 \pm 1.0 \pm 0.9$	11	10
160–180	2.16 ± 0.06	$6.3 \pm 0.9 \pm 0.8$	15	13
180–200	1.28 ± 0.04	$6.0 \pm 1.5 \pm 0.8$	25	14
200–230	0.66 ± 0.03	$2.8 \pm 0.8 \pm 1.5$	27	55
230–260	0.34 ± 0.02	$1.32 \pm 0.47 \pm 0.06$	35	5
260–290	0.15 ± 0.01	$0.33 \pm 0.14 \pm 0.03$	41	10
290–350	0.044 ± 0.005	–	–	–
350–450	0.007 ± 0.001	–	–	–

Table 20 Double differential cross section in kinetic energy bins at production (E^p_{kin}) of protons produced by 221 MeV/u ^{12}C ion beam impinging on a PMMA target, detected at 90° (top panel) and 60° (bottom panel). The production cross section from the FLUKA Monte Carlo simulation (*MC*) is listed alongside the experimental cross section (*data*), with the relative statistical and systematic data uncertainties reported as percentage in the last two columns

E^p_{kin} [MeV]	$\frac{d^2\sigma^{MC}}{d\Omega dE_k}$ [b/sr/MeV]	$\frac{d^2\sigma^{data}}{d\Omega dE_k}$ [b/sr/MeV]	Δ^{data}_{stat} [%]	Δ^{data}_{sys} [%]
90°	$\times 10^{-4}$	$\times 10^{-4}$		
40–60	24.2 ± 0.2	$23.8 \pm 1.0 \pm 1.0$	4	4
60–80	12.0 ± 0.1	$12.9 \pm 0.7 \pm 0.9$	6	7
80–100	5.88 ± 0.09	$6.9 \pm 0.6 \pm 0.4$	9	6
100–120	2.92 ± 0.06	$3.3 \pm 0.4 \pm 0.3$	11	9
120–140	1.64 ± 0.05	$1.7 \pm 0.3 \pm 0.2$	16	13
140–180	0.66 ± 0.02	$0.8 \pm 0.2 \pm 0.2$	21	30
180–250	0.147 ± 0.007	$0.09 \pm 0.03 \pm 0.03$	32	28
250–350	0.013 ± 0.002	–	–	–
60°	$\times 10^{-4}$	$\times 10^{-4}$		
40–60	124.7 ± 0.4	$101 \pm 2 \pm 6$	2	6
60–80	92.8 ± 0.4	$97 \pm 2 \pm 6$	2	6
80–100	64.5 ± 0.3	$69 \pm 2 \pm 3$	3	5
100–120	39.2 ± 0.2	$47 \pm 2 \pm 2$	3	5
120–140	21.4 ± 0.2	$37 \pm 2 \pm 2$	5	5
140–160	10.8 ± 0.1	$25 \pm 2 \pm 3$	7	11
160–180	5.49 ± 0.09	$22 \pm 2 \pm 4$	10	20
180–200	3.06 ± 0.07	$13 \pm 2 \pm 5$	13	37
200–230	1.51 ± 0.04	$9 \pm 2 \pm 3$	17	35
230–260	0.70 ± 0.03	$15 \pm 6 \pm 5$	40	34
260–290	0.35 ± 0.02	$3.2 \pm 1.1 \pm 0.7$	35	23
290–350	0.137 ± 0.008	$0.7 \pm 0.2 \pm 0.2$	29	26
350–450	0.027 ± 0.003	$0.3 \pm 0.2 \pm 0.2$	69	61

Table 21 Double differential cross section in kinetic energy bins at production (E^p_{kin}) of protons produced by 279 MeV/u ^{12}C ion beam impinging on a PMMA target, detected at 90° (top panel) and 60° (bottom panel). The production cross section from the FLUKA Monte Carlo simulation (*MC*) is listed alongside the experimental cross section (*data*), with the relative statistical and systematic data uncertainties reported as percentage in the last two columns

E^p_{kin} [MeV] 90°	$\frac{d^2\sigma^{MC}}{d\Omega dE_k}$ [b/sr/MeV] $\cdot 10^{-4}$	$\frac{d^2\sigma^{data}}{d\Omega dE_k}$ [b/sr/MeV] $\cdot 10^{-4}$	Δ^{data}_{stat} [%]	Δ^{data}_{sys} [%]
40 - 60	29.9 ± 0.2	$28 \pm 1 \pm 1$	4	5
60 - 80	15.1 ± 0.2	$16.4 \pm 0.9 \pm 0.7$	6	4
80 - 100	7.7 ± 0.1	$9.4 \pm 0.8 \pm 0.5$	8	6
100 - 120	4.28 ± 0.08	$4.8 \pm 0.5 \pm 0.2$	10	5
120 - 140	2.15 ± 0.06	$3.4 \pm 0.6 \pm 0.9$	17	25
140 - 180	0.83 ± 0.03	$1.3 \pm 0.3 \pm 0.2$	19	12
180 - 250	0.164 ± 0.009	$0.30 \pm 0.09 \pm 0.04$	31	12
250 - 350	0.015 ± 0.002	-	-	-
60°	$\cdot 10^{-4}$	$\cdot 10^{-4}$		
40 - 60	140.5 ± 0.5	$101 \pm 2 \pm 7$	2	7
60 - 80	112.2 ± 0.5	$105 \pm 2 \pm 7$	2	7
80 - 100	87.4 ± 0.4	$80 \pm 2 \pm 4$	2	6
100 - 120	62.5 ± 0.3	$60 \pm 2 \pm 3$	3	5
120 - 140	40.3 ± 0.3	$44 \pm 2 \pm 3$	4	8
140 - 160	24.0 ± 0.2	$36 \pm 2 \pm 2$	5	5
160 - 180	13.9 ± 0.2	$31 \pm 2 \pm 3$	7	10
180 - 200	7.7 ± 0.1	$22 \pm 2 \pm 3$	10	12
200 - 230	3.83 ± 0.07	$17 \pm 2 \pm 7$	12	41
230 - 260	1.70 ± 0.05	$10 \pm 2 \pm 5$	17	46
260 - 290	0.78 ± 0.03	$4.5 \pm 1.0 \pm 1.6$	22	35
290 - 350	0.26 ± 0.01	$1.8 \pm 0.5 \pm 0.7$	27	40
350 - 450	0.040 ± 0.004	-	-	-

Table 22 Double differential cross section in kinetic energy bins at production (E^p_{kin}) of protons produced by 351 MeV/u ^{12}C ion beam impinging on a PMMA target, detected at 90° (top panel) and 60° (bottom panel). The production cross section from the FLUKA Monte Carlo simulation (*MC*) is listed alongside the experimental cross section (*data*), with the relative statistical and systematic data uncertainties reported as percentage in the last two columns

E^p_{kin} [MeV]	$\frac{d^2\sigma^{MC}}{d\Omega dE_k}$ [b/sr/MeV]	$\frac{d^2\sigma^{data}}{d\Omega dE_k}$ [b/sr/MeV]	Δ^{data}_{stat} [%]	Δ^{data}_{sys} [%]
90°	$\times 10^{-4}$	$\times 10^{-4}$		
40–60	33.8 ± 0.2	$32 \pm 1 \pm 1$	4	4
60–80	19.0 ± 0.2	$19.9 \pm 1.0 \pm 1.1$	5	6
80–100	10.4 ± 0.1	$11.2 \pm 0.7 \pm 0.7$	6	6
100–120	6.06 ± 0.09	$8.2 \pm 0.7 \pm 0.4$	9	5
120–140	3.43 ± 0.07	$5.0 \pm 0.6 \pm 0.2$	12	4
140–180	1.43 ± 0.03	$2.0 \pm 0.2 \pm 0.3$	12	14
180–250	0.30 ± 0.01	$0.6 \pm 0.1 \pm 0.2$	22	24
250–350	0.026 ± 0.003	–	–	–
60°	$\times 10^{-4}$	$\times 10^{-4}$		
40–60	136.1 ± 0.5	$97 \pm 2 \pm 5$	2	5
60–80	117.8 ± 0.4	$107 \pm 2 \pm 6$	2	5
80–100	100.8 ± 0.4	$89 \pm 2 \pm 6$	2	6

Table 22 continued

E^{p}_{kin} [MeV]	$\frac{d^2\sigma^{MC}}{d\Omega dE_k}$ [b/sr/MeV]	$\frac{d^2\sigma^{data}}{d\Omega dE_k}$ [b/sr/MeV]	Δ^{data}_{stat} [%]	Δ^{data}_{sys} [%]
100–120	80.7 ± 0.4	$65 \pm 2 \pm 3$	2	5
120–140	60.6 ± 0.3	$55 \pm 2 \pm 4$	3	7
140–160	41.1 ± 0.3	$45 \pm 2 \pm 4$	4	9
160–180	26.8 ± 0.2	$36 \pm 2 \pm 2$	4	5
180–200	17.1 ± 0.2	$33 \pm 2 \pm 4$	6	12
200–230	9.3 ± 0.1	$29 \pm 2 \pm 11$	8	39
230–260	4.70 ± 0.07	$17 \pm 2 \pm 3$	10	18
260–290	2.42 ± 0.05	$10 \pm 1 \pm 1$	13	14
290–350	0.91 ± 0.02	$3.7 \pm 0.5 \pm 1.5$	14	40
350–450	0.165 ± 0.007	$2.3 \pm 1.0 \pm 1.0$	44	43
450–650	0.007 ± 0.001	–	–	–

Table 23 Energy integrated differential cross section of protons produced by ^{12}C ion beam of kinetic energy (E^{C}_{kin}) ranging from 115 MeV/u to 351 MeV/u impinging on a PMMA target. Protons are detected at 90° (top panel) and 60° (bottom panel). The production cross section from the FLUKA Monte Carlo simulation (*MC*) is listed alongside the experimental cross section (*data*), with the relative statistical and systematic data uncertainties reported as percentage in the last two columns

E^{C}_{kin} [MeV/u]	$\frac{d\sigma^{MC}}{d\Omega}$ [b/sr]	$\frac{d\sigma^{data}}{d\Omega}$ [b/sr]	Δ^{data}_{stat} [%]	Δ^{data}_{sys} [%]
90°	$\times 10^{-2}$	$\times 10^{-2}$		
115	5.01 ± 0.04	$3.8 \pm 0.2 \pm 0.2$	4	4
150	6.49 ± 0.04	$6.0 \pm 0.2 \pm 0.3$	4	4
221	9.70 ± 0.05	$10.1 \pm 0.3 \pm 0.4$	3	4
279	12.28 ± 0.06	$12.9 \pm 0.4 \pm 0.5$	3	4
351	15.32 ± 0.07	$16.4 \pm 0.4 \pm 0.7$	2	4
60°	$\times 10^{-1}$	$\times 10^{-1}$		
115	3.61 ± 0.01	$3.92 \pm 0.06 \pm 0.16$	2	4
150	3.74 ± 0.01	$5.40 \pm 0.08 \pm 0.23$	1	4
221	7.32 ± 0.01	$8.32 \pm 0.09 \pm 0.43$	1	5
279	9.98 ± 0.02	$10.0 \pm 0.1 \pm 0.5$	1	5
351	12.17 ± 0.02	$11.7 \pm 0.1 \pm 0.6$	1	5

Table 24 Energy integrated differential cross section of deuterons produced by ^{12}C ion beam of kinetic energy (E^{C}_{kin}) ranging from 115 MeV/u to 351 MeV/u impinging on a PMMA target. Deuterons are detected at 90° (top panel) and 60° (bottom panel). The production cross section from the FLUKA Monte Carlo simulation (*MC*) is listed alongside the experimental cross section (*data*), with the relative statistical and systematic data uncertainties reported as percentage in the last two columns

E^{C}_{kin} [MeV/u]	$\frac{d\sigma^{MC}}{d\Omega}$ [b/sr]	$\frac{d\sigma^{data}}{d\Omega}$ [b/sr]	Δ^{data}_{stat} [%]	Δ^{data}_{sys} [%]
90°	$\times 10^{-3}$	$\times 10^{-3}$		
115	1.92 ± 0.07	$0.8 \pm 0.2 \pm 0.1$	23	14
150	7.2 ± 0.1	$2.1 \pm 0.3 \pm 0.1$	14	7
221	13.2 ± 0.2	$4.1 \pm 0.4 \pm 0.3$	9	8
279	12.1 ± 0.2	$8.1 \pm 0.8 \pm 0.4$	10	5
351	10.9 ± 0.2	$10.3 \pm 1.0 \pm 1.0$	10	10
60°	$\times 10^{-2}$	$\times 10^{-2}$		
115	4.75 ± 0.04	$3.5 \pm 0.2 \pm 0.3$	5	8
150	4.88 ± 0.04	$6.0 \pm 0.3 \pm 0.4$	4	7
221	5.10 ± 0.04	$10.3 \pm 0.4 \pm 0.7$	4	6
279	4.12 ± 0.04	$13.1 \pm 0.7 \pm 0.7$	5	6
351	3.41 ± 0.03	$12.0 \pm 0.6 \pm 0.7$	5	6

Table 25 Energy integrated differential cross section of tritons produced by ^{12}C ion beam of kinetic energy (E^C_{kin}) ranging from 115 MeV/u to 351 MeV/u impinging on a PMMA target. Tritons are detected at 60°. The production cross section from the FLUKA Monte Carlo simulation (*MC*) is listed alongside the experimental cross section (*data*), with the relative statistical and systematic data uncertainties reported as percentage in the last two columns. Cross section for tritons detected at 90° is not reported due to insufficient statistics

E^C_{kin} [MeV/u]	$\frac{d\sigma^{MC}}{d\Omega}$ [b/sr]	$\frac{d\sigma^{data}}{d\Omega}$ [b/sr]	Δ^{data}_{stat} [%]	Δ^{data}_{sys} [%]
60°	$\times 10^{-3}$	$\times 10^{-3}$		
115	3.25 ± 0.10	$2.9 \pm 0.6 \pm 0.7$	19	23
150	4.6 ± 0.1	$5.9 \pm 0.9 \pm 0.8$	15	14
221	6.1 ± 0.1	$13.6 \pm 1.6 \pm 0.9$	12	6
279	5.1 ± 0.1	$22 \pm 4 \pm 5$	17	20
351	4.1 ± 0.1	$15 \pm 2 \pm 4$	16	23

References

1. M. Durante et al., Charged-particle therapy in cancer: clinical uses and future perspectives. Nat. Rev. Clin. Oncol. **14**(8), 483–495 (2017)
2. M. Durante, H. Paganetti, Nuclear physics in particle therapy: a review. Rep. Prog. Phys. **79**, 096702 (2016)
3. S. Muraro et al., Monitoring of hadrontherapy treatments by means of charged particle detection. Front. Oncol. **6**, 177 (2016)
4. M. Durante, F.A. Cucinotta, Physical basis of radiation protection in space travel. Rev. Mod. Phys. **83**, 1245 (2011)
5. M. Durante, Space radiation protection: destination mars. Life Sci. Sp. Res. (Amst) **1**, 2–9 (2014)
6. F. Tommasino, M. Durante, Proton radiobiology. Cancers (Basel) **7**(1), 353–81 (2015)
7. S. Muraro, G. Battistoni, A.C. Kraan, Challenges in Monte Carlo simulations as clinical and research tool in particle therapy: a review. Front. Phys. (2020). https://doi.org/10.3389/fphy.2020.567800
8. W. Webber, J. Kish, D. Schrier, Individual charge changing fragmentation cross sections of relativistic nuclei in hydrogen, helium, and carbon targets. Phys. Rev. C **41**(2), 533–546 (1990). https://doi.org/10.1103/physrevc.41.533
9. J. Dudouet et al., Double-differential fragmentation cross-section measurements of 95 MeV/nucleon ^{12}C beams on thin targets for hadron therapy. Phys. Rev. C **88**, 024606 (2013). https://doi.org/10.1103/PhysRevC.88.024606
10. J. Dudouet et al., Zero-degree measurements of ^{12} C fragmentation at 95 MeV/nucleon on thin targets. Phys. Rev. C **89**, 064615 (2014). https://doi.org/10.1103/PhysRevC.89.064615
11. C. Zeitlin et al., Fragmentation of ^{14} N,^{16}O,^{20}Ne, and ^{24}Mg nuclei at 290 to 1000 MeV/nucleon. Phys. Rev. C **83**, 034909 (2011). https://doi.org/10.1103/PhysRevC.83.034909
12. R. Pleskac, et al., (FIRST collaboration), The FIRST experiment at GSI. Nucl. Instrum. Methods A 678, 130–138 (2012) https://doi.org/10.1016/j.nima.2012.02.020
13. M. Toppi, et al., (First collaboration), Measurement of fragmentation cross sections of ^{12}c ions on a thin gold target with the first apparatus. Phys. Rev. C **93**(6), 064601 (2016). https://doi.org/10.1103/PhysRevC.93.064601
14. C. Divay et al., Differential cross section measurements for hadron therapy: 50 mev/nucleon ^{12}c reactions on h, c, o, al, and ^{nat}ti targets. Phys. Rev. C **95**(4), 044602 (2017). https://doi.org/10.1103/PhysRevC.95.044602
15. https://eljentechnology.com/images/products/data_sheets/EJ-200_EJ-204_EJ-208_EJ-212.pdf
16. I. Mattei et al., Measurement of 12-c fragmentation cross sections on c, o and h in the energy range of interest for particle therapy applications. IEEE Trans. Radiat. Plasma Med. Sci. **4**, 269–82 (2020)
17. G. Battistoni, M. Toppi, V. Patera et al., Measuring the impact of nuclear interaction in particle therapy and in radio protection in space: the FOOT experiment. Front. Phys. 8, 568242 (2021)
18. T. Bohlen et al., The fluka code: developments and challenges for high energy and medical applications. Nucl. Data Sheets **120**, 211–214 (2014)
19. G. Battistoni et al., The FLUKA code: An accurate simulation tool for particle therapy. Front./Oncol. **6**, 116 (2016)
20. S. Agostinelli, J. Allison et al., Geant4-a simulation toolkit. Nucl. Instrum. Methods Phys. Res. Sect. A **506**(3), 250–303 (2003). https://doi.org/10.1016/S0168-9002(03)01368-8
21. J. Allison et al., Geant4 developments and applications. IEEE Trans. Nucl. Sci. **53**(1), 270–278 (2006). https://doi.org/10.1109/TNS.2006.869826
22. J. Allison et al., Recent developments in geant4. Nuclear Instrum. Methods Phys. Res. Sect. A Acc. Spectrom. Detectors Assoc. Equip. **835**, 186–225 (2016). https://doi.org/10.1016/j.nima.2016.06.125
23. C.P. Karger et al., Dosimetry for ion beam radiotherapy. Phys. Med. Biol. **55**, 193–234 (2010)
24. P. Andreo et al.: IAEA TRS-398. IAEA (2006)
25. M. Donetti et al.: Private communication. CNAO (2019)
26. T. Adye, Unfolding algorithms and tests using RooUnfold. PHYSTAT 2011 Workshop, CERN, Geneva, Switzerland, January 2011, CERN-2011-006, 313–318 (2011)
27. R. Brun, F. Rademakers, Unfolding algorithms and tests using roounfold. Nucl. Instrum. Methods A **389**, 81 (1997)
28. M. Toppi et al., Monitoring carbon ion beams transverse position detecting charged secondary fragments: results from patient treatment performed at CNAO. Front. Oncol. (2021). https://doi.org/10.3389/fonc.2021.601784
29. M. Fischetti et al., Inter-fractional monitoring of ^{12}C ions treatments: results from a clinical trial at the CNAO facility. Sci. Rep. (2020). https://doi.org/10.1038/s41598-020-77843-z
30. L. Piersanti et al., Measurement of charged particle yields from pmma irradiated by a 220 mev/u ^{12}c beam. Phys. Med. Biol. **59**(7), 1857 (2012)
31. M. Marafini et al., Secondary radiation measurements for particle therapy applications: nuclear fragmentation produced by 4-he ion beams in a pmma target. Phys. Med. Biol. **62**(4), 1291–1309 (2017). https://doi.org/10.1088/1361-6560/aa5307
32. A. Rucinski et al., Secondary radiation measurements for particle therapy applications: charged particles produced by 4-He and 12-

C ion beams in a PMMA target at large angle. Phys. Med. Biol. (2018). https://doi.org/10.1088/1361-6560/aaa36a
33. A. Rucinski et al., Secondary radiation measurements for particle therapy applications: charged secondaries produced by 16-o ion beams in a PMMA target at large angles. Phys. Med.-Eur. J. Med. Phys. **64**, 45–53 (2019). https://doi.org/10.1016/j.ejmp.2019.06.001
34. F. Ballarini et al., The fluka code: overview and new developments. EPJ Nucl. Sci. Technol. **10**, 16 (2024)
35. M. Cavinato, E. Fabrici, E. Gadioli, E. Gadioli Erba, E. Risi, Boltzmann master equation theory of angular distributions in heavy-ion reactions. Nucl. Phys. A **643**, 15–29 (1998)
36. H. Sorge, H. Stocker, W. Greiner, Relativistic quantum molecular dynamics approach to nuclear collisions at ultrarelativistic energies. Nucl. Phys. A **498**(3), 567–576 (1989)
37. H. Sorge, Flavor production in pb(160 a gev) on pb collisions: effect of color ropes and hadronic rescattering. Phys. Rev. C **52**, 3291–3314 (1995)
38. G. Folger, V.N. Ivanchenko, J.P. Wellisch, The binary cascade - nucleon nuclear reactions. Eur. Phys. J. A **21**, 407 (2004). https://doi.org/10.1140/epja/i2003-10219-7
39. D. Mancusi, K. Niita, T. Maruyama, L. Sihver, Stability of nuclei in peripheral collisions in the jaeri quantum molecular dynamics model. Phys. Rev. C **79**, 014614 (2009). https://doi.org/10.1103/PhysRevC.79.014614
40. D. Mancusi, A. Boudard, J. Cugnon, J.-C. David, P. Kaitaniemi, S. Leray, Extension of the liège intranuclear-cascade model to reactions induced by light nuclei. Phys. Rev. C **90**, 054602 (2014). https://doi.org/10.1103/PhysRevC.90.054602